1-1-2013

Modeling Ultrasonic field Emanating from Scanning Acoustic Microscope for Reliable Characterization of Pathogens (Biological Materials)

Rowshan Ara Rima
University of South Carolina - Columbia

Modeling Ultrasonic field emanating from Scanning Acoustic Microscope for Reliable Characterization of Pathogens (Biological Materials)

by

Rowshan Ara Rima

Bachelor of Science
Bangladesh University of Engineering & Technology, 2009

Submitted in Partial Fulfillment of the Requirements

For the Degree of Master of Science in

Mechanical Engineering

College of Engineering and Computing

University of South Carolina

2014

Accepted by:

Sourav Banerjee, Director of Thesis

Victor Giurgiutiu, Reader

Lacy Ford, Vice Provost and Dean of Graduate Studies

DEDICATION

This work is dedicated to my parents: Dr. A. K. M. Rezaul Karim and Rokeya Karim,

and my husband: Dr. Md. Ershadul Alam

ACKNOWLEDGEMENTS

I would like to express my sincere appreciation and respect to my advisor Dr. Sourav Banerjee. His patience and guidance during my masters' study made it possible for the successful completion of this research. Without his invaluable advice and immeasurable amount of time spent with care for me, I would not be where I am today. It has been a true privilege and honor for me to work with Dr. Banerjee and I'm forever grateful to him.

I would like to thank Professor Anindya Chanda for providing the fungal specimen to perform scanning under SAM.

I would also like to thank my colleague, Riaz Ahmed, for his constant support and help throughout the program.

Finally, I would like to express my gratitude to family and friends for their support, constant encouragement and unconditional love to me.

ABSTRACT

Acoustic microscopy provides extraordinary advantages over state-of-the-art invasive imaging techniques to determine the mechanical properties of living colonies of pathogens and micro-organisms. It is possible to obtain the morphomechanical parameters of the pathogenic colonies e.g. variation of thickness, stiffness and the coefficients of attenuation, using scanning acoustic microscope (SAM). However, the process requires an expert with extensive understanding of SAM and ultrasonic signals which is very time consuming and expensive for complex form of analysis. Due to lack of a suitable computational tool, presently the ultrasonic wave scattering, reflection and transmission through the biological specimens cannot be properly visualized. Without any reliable simulated environment, it is extremely difficult to extract the morphomechanical parameters from the invading pathogens. To understand the ultrasonic signals that are reflected or scattered back from the biological specimens, one would need to compute the Pupil Function (PF), i.e. generated by a particular SAM lens. PF is the total pressure field in front of the lens at focal plane generated by the lens and cannot be experimentally measured without placing a reflecting surface in front of the lens. Hence to determine the PF one could change the interpretation of PF. Thus a detailed computer simulation platform for the SAM experiments is necessary. Particularly it is mandatory to obtain the accurate PF that is generated by a particular SAM lens used in the experiments before decoding the morphomechanical properties of the biological specimens.

To obtain the accurate PF in front of an acoustic lens, this dissertation presents a detailed development of Distributed Point Source Method (DPSM) for modeling SAM experiments. The ultrasonic field in front of the focused 100 MHz lens, obtained from the simulation can be further used to determine the material properties of the biological specimens. An accurate modelling of SAM lens using the distributed point source method (DPSM) is proposed for its proven capability to simulate ultrasonic fields at higher frequencies. DPSM is computationally cheap and efficient than the Finite Element Method (FEM).

The acoustic lenses used in the SAM are commonly made of sapphire but enclosed with a brass casing. The sapphire head consists of four different geometrical shapes and each segment has individual influences on the visualization of the ultrasonic field produced by the transducer. Thus, the accurate geometry of the acoustic lens is an important factor for modeling. Using the DPSM accurate geometry of a 100 MHz lens is modeled and the PF is computed in front of the lens. It is shown that as per the design specification of the lens, the pressure field is accurately focused at the focal point. The peak pressure at the focal point and the rippled wave effect away from the focal point are verified in the DPSM based simulation environment.

TABLE OF CONTENTS

LIST OF FIGURES

LIST OF SYMBOLS

ρ	Mass density
$\delta(x-y)$	Dirac-delta function
δ_{ij}	Kronecker delta function
ε_{ij}	Strain tensor
ε_{ijk}	Permutation symbol
σ_{ij}	Stress component
λ	Lame's first constant
μ	Lame's second constant
θ	Angle of rotation
ω	Angular (radial) frequency (rad/s)
ω_{ij}	Rotation tensor
ϕ	Scalar potential
Φ	Irrotational vector potential
ψ	Scalar potential
Ψ	Solenoidal vector potential

A	Source strength vector
A_S	Source strength vector representing surface S
A_m	Amplitude of m-th point source
C_{ijkl}	Stiffness tensor
C_p	Longitudinal (P) wave speed
C_s	Transverse (S) wave speed
f	Body force
G, G^*, G_{ij}	Green's function
k_f	Wave number in fluid media
L,M	Number of target points
N	Normal direction matrix
P	Magnitude of force vector with no temporal or spatial dependence
Pr	Pressure vector
Pr_S	Pressure vector at the excitation source surface S
R	Distance between a point source and a target point
r^*	Distance between a source point y and a target point x^*
r_m	distance between the m-th point source to a target point x
S	Surface area
S_{ij}	Stress component
t	Time

u	Displacement
u_i	i-th component of displacement
U_i	Spatial part of the displacement vector
v	Velocity vector
V_s	Velocity vector at the excitation source surface S
V_T	Velocity vector at the target points
V	Volume
X	Location of a target point
x_s	Arbitrary point on the surface S
x_m, y_m	Coordinates of the m-th point source

LIST OF ABBREVIATIONS

CSR ..... Controlled Space Radiation

DPSM ..... Distributed Point Source Method

SH wave ..... Shear Harmonic wave

SAM ..... Scanning Acoustic Microscope

FEM ..... Finite Element Method

CHAPTER 1

INTRODUCTION

1.1.Background and Motivation

The term pathogens has been used for an infectious agent, or a microorganism, in the widest sense such as virus, prion, bacteria or fungus, that causes disease to its host by secreting toxic agents. Bioactive chemicals discharged by the pathogens, such as *Aspergillus* fungi, can cause detrimental effect on human, animal and plant health, as well as food, nutrition and economy worldwide. *Aspergillus* spores are found nearly everywhere, so all the living animals and plants are almost constantly exposed to them. Generally, such exposures are normal, and pose no adverse effect on health condition. But, a recent study has found that, *Aspergillus* can and does cause diseases though the production of mycotoxins. The most common pathogenic species of *Aspergillus* is *Apergillus flavus*, and it produces aflatoxin, which is both a toxin and a carcinogen, and can potentially contaminate foods[1-13]. Figure 1.1 shows the photographic image [Ref: figure 1] of the detrimental effect of *Aspergillus flavus*. Similarly *Aspergillues paraciticus* which is another fungal species produces carcinogenic aflatoxin in to the air corrupting our indoor air quality. It is reported that in the US alone the mycotxin management cost is annually $1.3 – $ 2.5 billon[10] which involves chemical treatment. Thus there is an opportunity exists to find an alternative approach to control aflatoxin (a form of mycotoxin) by an alternative cheaper menas using mechanical interventions via ultrasonics. Thus it is necessary to understand their mechanical characteristics.

Figure 1.1: Detrimental effect of *Aspergillus* Fungus on food

Significant research effort has been made to understand about the mechanism of secretion of the toxin chemicals and their relation to the biological behavior of the source pathogens. Also, researchers are interested to know the growth pattern of the *Aspergillus* colony and the degrees of mechanochemical forces that are exerted by the *Aspergillus* which helps them to penetrate the host body and extract nutrient. It has been hypothesized that, for maximization of the toxin production, the *Aspergillus* has a synchronized form of action which consists of significant mechanical transformation before, during and after the toxin secretion. If this hypothesis is true and the mechanism is known, appropriate mechanical means (non-chemical and thus eco-friendly) could be taken to interrupt the process. Thus, the knowledge of the time-dependent mechanical properties is important to understand the mechanical behavior of the *Aspergillus.*

1.2 Limitations of state-of-the-art techniques

Optical microscopy has been used to determine the biological behavior of pathogens. However, the mechanical properties cannot be obtained by using this method. Determination of the mechanical properties of pathogens (or any living cells) is a difficult task. Different techniques, such as, local aspiration of cytoplasm with a pipette, local

poking of cytoplasm, magnetometry, or scanning force microscopy had been used by various investigators. Aforementioned methods measure the forces that are needed to evoke a certain deformation in the cells. From the stress-strain relationships, these invasive methods determine the visco-elastic properties of the specimen and oscillating stress as a function of frequency. Among all the methods, acoustic microscopy provides some extraordinary advantages (provides excellent spatial resolution, relatively fast and is minimally invasive) to determine the mechanical properties of pathogens.

There are other benefits of using the acoustic waves in microscopy technology. One important aspect of using the acoustic wave is that, it has the ability to inspect a specimen in dark region; the situation is often needed for the biological specimens. Another aspect of using the acoustic wave is its ability to see inside the optically opaque specimen, which is the main reason for the popularity of acoustic waves in electronic packaging industries for inspecting the integrated circuit (IC) chips.

1.3 Limitation of SAM

For biological cell characterization, normally 100 MHz to 1 GHz ultrasound frequencies are used. Two different types of fungal colonies named *Aspergillues paraciticus* and *Aspergillus niger* were inspected and it was found that their morphological characteristics are very different (see Fig.1.2). A highly customized SAM 300 microscope manufactured by PVATepla, Germany was used for acoustic imaging. Although the SAM technology is quite advanced it was identified that there are significant opportunities exists for improving the methods of understanding the acoustic signals emanating from SAM and subsequently determine the mechano-morphological

parameters of pathogenic colonies. In order to quantify such characteristics, first it is necessary to perform accurate modeling of SAM experiments to understand ultrasonic wave that are reflected and scattered by the biological specimens. No such detailed modeling exists that can provide accurate pupil function in front of a SAM lens.

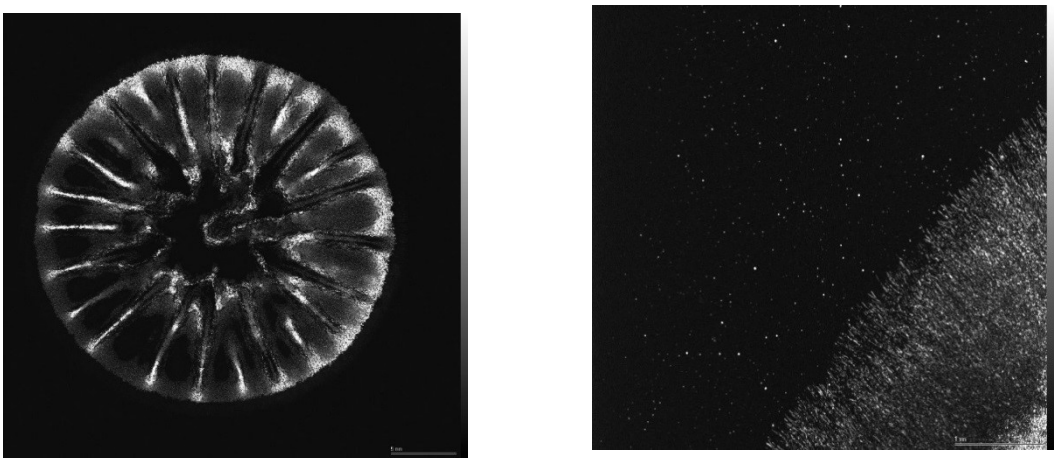

Figure 1.2 SAM 100 MHz images of *Aspergillus paraciticus* colony with propagating hyphae

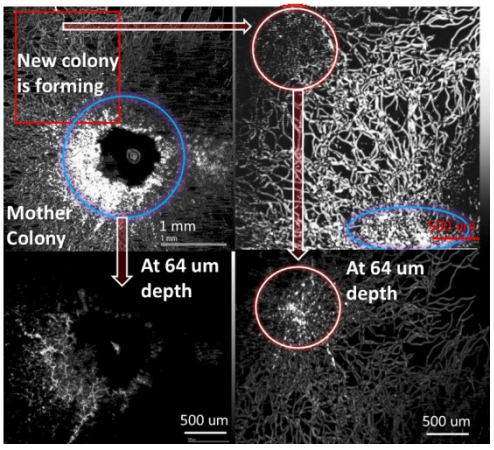

Figure 1.3 SAM 100 MHz transducer image of *Aspergillus niger* colony at different depth, showing in depth hyphal network

1.4 Definition of Pupil Function

In acoustic microscopy experiments, V(f) and V(z) techniques are used to measure the elastic wave speed and the attenuation of wave. These plots are the variation of ultrasonic signal voltage (V) as a function of the frequency of signal (f) and defocus distance (z). The voltage detected by these techniques (due to wave field propagating in the positive direction and the reflected wave field coming back from the substrate) can be written as:

$$V(z) = \int_{-\infty}^{\infty}\int_{-\infty}^{\infty} P\big(k_x, k_y, z\big)P\big(-k_x, k_y, z\big)R(k_x, k_y, z)e^{\frac{(i2k_z z)}{abs(k)k_z}}dk_x dk_y$$

Similarly,

$$V(f) = \int_{-\infty}^{\infty}\int_{-\infty}^{\infty} P\big(k_x, k_y, F, f\big)P\big(-k_x, k_y, F, f\big)R(f)e^{\frac{(i2k_z F)}{abs(k)k_z}}dk_x dk_y$$

Where, P is the Pupil function, F is the focal distance, f is frequency and R is the reflection coefficient. The Pupil function P can be written as:

$$P\big(k_x, k_y, z\big) = \int_{-\infty}^{\infty}\int_{-\infty}^{\infty} \Phi(x, y, z)e^{(-ik_x x - ik_y y)}dxdy$$

For pupil function, it is standard to assume or calculate by fitting a polynomial function through several experiments. But, polynomial fit might not represent the actual properties of the wave field in front of the lens. Hence, in order to estimate the wave speed and the attenuation of the specimen, a semi-analytical method called DPSM has been used to model a 100 MHz acoustic microscope lens. This predicted pressure field generated by the model can be used to compute the thickness profile and the properties of the pathogen from the experimental data. However, obtaining the mechano-

morphological parameters of our model pathogen (*Aspergillus paraciticus*) would be the next step and was not conducted under the activity of this thesis.

1.5 Problem description and Objective

The objective of this problem is to model the ultrasonic field generated by ultrasonic transducers of finite dimension when the transducer are immersed partially on a fluid. Thus, it numerically simulates the pupil function and focusing of the ultrasonic beam emanating from SAM transducers, which can be further used for the cell property determination.

Broadband acoustic lens centered at 100 MHz was used for *Aspergillus* imaging. Hence, in this study, a 100 MHz acoustic lens has been accurately modeled using the actual geometric configuration (Refer Chapter 5). To model the sample 100 MHz lens, DPSM technique has been used and the source strength is given accurately on the transducer position which is located at the top surface of the lens rod. Fundamentally the pupil function, which is our target to find using the proposed model, cannot be accurately determined from any experiments. Because the Pupil function is the pure pressure field generated by the particular lens in absence of any reflecting surface in front. However, any experiment that can be conducted requires a reflecting surface. So with the intention of measuring pupil function once could alter the pupil function that is measured. Traditional approach to determine the pupil function is to assume a quadratic function of depth or frequency. Using multiple reflection data from the experiments and followed by an error minimization scheme the pupil function is obtained. As it is argued the state-of-

the-art method is not accurate, This thesis contribute an accurate calculation of pupil function by modeling a 100 MHz SAM lens using DPSM.

CHAPTER 2

LITERATURE REVIEW

2.1 Acoustics

The advancement of the theory of acoustics is closely related to advances in solid mechanics [14, 15]. Classical mechanics, including acoustic phenomena, was first inquired by Galileo around 1640. Robert Hook investigated the frequency and pitch of vibration and elasticity in the quasi-static state in the late 17^{th} century, and the mathematical foundation for the dynamic expression of materials was established by Issac Newton. In the early 19^{th} century, Thomas Young introduced the concept of a modulus as a material property for elastic deformation. Navier brought to light the general form of the equation of equilibrium and the equation of motion for a body under elastic deformation in 1821. A year later, Navier's oversimplified assumption was corrected by Cauchy and equations for isotropic materials were determined with displacements as independent variables. The extensions of these equations for anisotropic materials were made in 1828. Using energy considerations of an elastic body, the equation of motion for anisotropic materials had also been derived by George Green. He also accurately determined the number of necessary independent coefficients [16].

Lord Rayleigh has a significant contribution in the field of acoustics. He examined thoroughly the elastic waves which propagate in a body along its surface [17, 18].

Horace Lamb was particularly interested in elastic waves whose particle motion lies in the plane that contains the direction of wave propagation and the plate normal (the direction perpendicular to the plate) [18, 19]. The major difference between Rayleigh and Lamb wave is the dispersive characteristics of the Lamb wave in a plate while the Rayleigh wave is non-dispersive in an elastic half space.

With the expansion of the energy methods in 19^{th} century, understanding of stress distributions in an elastic body has increased, and use of energy method has been obvious for dealing with vibrations. Pochammer [20] and Chree [21] independently worked on determining an exact solution to elastic harmonic wave propagation in cylindrical bars, and in doing so, they found a dispersion relation for longitudinal, torsional and flexural waves. This was a significant conclusion as it was contradictory to the analysis of simple longitudinal waves developed before. Wave propagation in solid media in cylindrical geometry has been investigated by many other researchers [22-26].

2.2 DPSM (Distributed Point Source Method)

Placko and Kundu was the pioneer of the distributed point source method (DPSM). It is a semi-analytical technique which was first used as a tool to model the electromagnetic field generated by a magnetic sensor. The theoretical framework of DPSM and its application for modeling ultrasonic field was introduced in 2001 by Placko and Kundu [27]. The method was extended to problems with an interface between media in the following year by Placko, Kundu and Ahmad [28]. Also, modeling is done for an ultrasonic field generated by a transducer when a finite dimension scatterer is present in

front of the transducer [29]. These works demonstrates the effectiveness of DPSM in modeling wave propagation in different media.

Prior to 2005, many more applied problems were solved using DPSM. Ahmad was the first to work on modeling of phased array transducers using DPSM [30]. After that, wave propagation in corrugated plates, in layered medium and in acoustic microscopy has been done by many researchers [15, 31-35].

The technique of DPSM has been modified further to suit with the real life problems. Mainly, the point source distribution is the major modification area. In 2003, rather than using elemental point sources, triplet sources were developed [29]. This modification was introduced for modeling a solid surface, for which, the source strength is a vector quantity rather than a scalar value as in the fluid medium. To specify the direction of radiation, controlled space radiation (CSR) sources were introduced additionally.

2.3 Transducers

There are two major approaches in the theoretical study of velocity and pressure fields produced by a rigid planar source in an infinite baffle. The first approach is based on the presumption that over the source surface the amplitude of excitation is non-uniform, and the other concerns transient or pulse excitation. In both approaches, to solve the baffled radiator problem, there are four mathematical methods employed—

1. Rayleigh surface integral, 2. King integral, 3. Schoch solution, and 4. Convolution integral.

In 1945, the Rayleigh surface integral is utilized first [17]. It is based on Huygens' Principle, which states "every point may be considered as the source of an outgoing spherical wavelet for a plane vibrating surface, and the field at an arbitrary point can be constructed from the superposition of these wavelets." The piston source can be of any arbitrary shape, and the velocity of source does not have to be uniform over the surface in the Rayleigh surface integral.

An alternative method came from King for a circular piston with sinusoidal excitation in 1934 [36]. In his publication, he considered only the uniform velocity distribution. However, the work was later extended to analyze the excitation with an arbitrary velocity distribution by Bouwkamp in 1946 [37]. The King integral can be obtained by several ways including the homogeneous Helmholtz equation and Rayleigh integral. The limiting factor is that, in the analysis, the integration is over an infinite domain.

In 1941, Schoch found a solution of the problem for an arbitrarily shaped planar source vibrating sinusoidally with uniform amplitude [38, 39]. Physically, the Schoch solution is a statement of diffraction phenomena, which bears explanation of diffraction by Thomas Young and differs from Huygens' view.

The convolution process can be used for clarification of the field produced by a planar piston. The method includes determining the spatial impulse response function that couples the acoustic fields to the source geometry. Analytically it is possible to determine the spatial impulse response function for a plane circular radiator [40-48].

2.3.1 Non-Uniform Excitation Amplitude Distribution

In the study of piston radiators, works done varies from one another on how the piston vibration is mathematically represented. Though a rigid planar piston with uniform vibration amplitude distribution is of academic interest, a non-uniform amplitude distribution is relevant for empirical applications since the operation of real-world transducers involves the periodic deformation of an elastic baffle, and does not allow the distribution of uniform amplitude across the surface. In general, the piston motion is predicted to be axisymmetric and has $\left(1-\frac{r_0^2}{a^2}\right)^n$ dependence such that at the center of piston the maximum amplitude occurs, and it decreases as the radial coordinate r_o increases [49, 50].

For the radiator with non-uniform excitation, the amplitude analysis usually involves the evaluation of either the Rayleigh or King integral for a harmonically oscillating circular disk. Many studies have been done to determine these integrals and the solutions for the far field and the piston surface [51-53]. The expression of the radiated field using Bessel functions was made by Guptill in early 50's [54].

Between mid-40's and mid-50's, the Rayleigh integral became the major hypothesis of the numerical analysis performed. The publications during this time varied in the analysis by manipulating the amplitude distribution and radiator shape. These studies include the effect of discontinuous piston amplitude on the far-field radiation characteristics [55], a numerical evaluation of the Rayleigh integral for the far-field pressure produced by pistons with different supports [56], and computations of the errors in measuring attenuation by using sinusoidal, Gaussian, and Fermi waveforms [57]. For

simply-supported and clamped pistons, on-axis and far-field distribution were calculated by Dekker [58]. This solution was an exact solution of the Rayleigh integral.

Greenspan presented the extended study of a piston with rigid, simply-supported, clamped, and Gaussian vibration distributions [50]. His solution was the same as Dekker's, and the expressions for all four cases were in terms of elementary functions. He also shortly discussed the intensity of a rigid piston. As will be mentioned in the next section, Greenspan also presented results on transient problems.

2.3.2 Transient Excitation

Another important area of the study of piston radiators was the transient field created by a pulsed radiator in a rigid infinite baffle. Prior to 1970, the variety of features concerning this type of excitation had been thoroughly reviewed by both Hanish [59] and Freedman [60].

Morse was the first to derive an approximate expression for the transient field produced by a circular piston in 1948 [61]. The study of transient excitation began with the analysis of either the Rayleigh or King integral at first. However, the convolution integral gained popularity after a more thorough explanation on how the impulse response function can express the acoustic field as a convolution integral by Oberhettinger [43].

By introducing the inverse Fourier transform of harmonic piston oscillation *i.e.* the spatial impulse response function the piston velocity, Fischer described the transient field generated by a planar piston in an arbitrary shape [48]. For a circular piston, the

impulse response first appeared in Miles' work in 1953 [42]. Although it was not recognized as an impulse response, he employed the Laplace transform and Bessel integral relationship to determine the solution for a pulsed circular piston.

Though it was not the conventional approach, the Schoch approach was used to determine the pressure in the time domain due to an arbitrary velocity distribution. The publication by Kozina and Makarov [39] was the first time the Schoch approach was used to create a solution in the time domain.

Between the mid-60's and mid-70's, several publications including the convolution integral representation has appeared; however, they addressed the solutions to particular problems rather than drawing attention to the convolution integral representation as a method. The convolution integral derived by Oberhettinger [43] was obtained by others through alternative methods by taking an suitable coordinate transformation of Rayleigh integral [62] as well as utilizing Laplace and Hankel transforms [63].

In 1967, Ferris found that a time-dependent Green's function can be utilized to describe a general expression for the pressure due to a concentrated acoustic source or sources [64]. He identified that the shape of a surface defining the source or sources and the position of the field point determine the impulse response function although he did not discuss any particular source arrangement.

Tupholme displayed how the appropriate Green's function can lead to the Rayleigh integral for a pulsed field due to a baffled planar radiator of any shape [65]. The paper by Chadwick and Tupholme [63] considered only a circular piston a few years

back. Tupholme, in his article, measured the solution and used it for the circular disk to infinite strip cans and infinite wedge pistons.

As described so far, prior to Stepanishen, several researchers had achieved to solutions for the field generated by a planar circular radiator. However, he was the first author to reach the results for a circular radiator via the convolution integral theory. He published three articles in 1971 [45-47]. Each of them had different concentration on different features of a planar piston in a rigid infinite baffle, oscillating at an arbitrary velocity distribution. Papadakis and Fowler demonstrated the pressure distribution created by a pulsed circular disk via summation of field at a single frequency [57]. Weight of a frequency was empirically determined.

A greater effort to apply and verify the solutions obtained in practical ways became obvious in the mid-70's. Researchers in this period started to incorporate more practical aspects into their research [40, 41].

Greenspan contributed to the research of transient excitation as well as the distribution of non-uniform velocity amplitude [50]. He derived the general King integral in order to incorporate the use of the integral to a circular radiator with non-uniform velocity amplitude as mentioned earlier. Through the analysis of his velocity potential expression, he obtained analytical solution for a radiator under four different conditions. In both transient and non-transient excitations, the recent aspiration is in identifying a simple yet precise and compact expression so that it can be integrated into numerical analysis.

A series solution for the velocity potential originated by circular piston is derived by Hasegawa, Inoue, and Matsuzawa [66]. The expression consists of a spherical Bessel function, a spherical Hankel function of the second kind, and a Legendre polynomial. The exact solutions published before this work had problem with computations at high frequencies [67] and were not legitimate on the piston surface [68]. The expression derived in this paper is valid at any field points such as the piston surface, and the sample numerical result is consistent with the analytical solutions.

In 2005, two series expansions were derived for pressure fields due to a baffled circular piston by expanding the integrand of the Rayleigh integral [69].

The outer expansion which is valid for the region $r \geq a$ (where *a* is the radius of the piston and *r* is the distance from the piston center) was previously published [53, 70]; however, none of them clearly presented series coefficients. Here, the author derived these coefficients. The outer expansion converges well except for $r \approx a$ and requires $N \sim ka$ order of terms for convergence. The paraxial expansion or near-field solution is valid for $\leq \sqrt{z^2 + a^2}$, where w and z are the perpendicular distance to and the distance along the piston axis, respectively. The region near the piston axis ($w = 0$) provides the fastest convergence while the convergence is the slowest at $\approx \sqrt{z^2 + a^2}$. The order of *N~kw* is necessary for convergence. These expansions are analytically and computationally straightforward and possess good convergence properties compared to the exact solution [71].

As an extension of the fast near-field method (FNM), Kelly and McGough developed an annular superposition method [72]. This method involves a numerical

integration of a double integral expression. The advantage of an annular superposition integral over the commonly used Rayleigh-Sommerfield integral and King integral is its much faster convergence. The method does not involve integration over an infinite domain compared to King integral. However, this is only applicable to axisymmetric/circular acoustic radiators.

Mellow derived pressure expressions due to a resilient disk in an infinite baffle [73] and in free space [74]. In the former publication, the canonical form (closed form) expressions for near-field, immediate near-field, and far-field pressure distributions due to a monopole circular source (resilient disk) in an infinite baffle are presented. The velocity distribution is arbitrary or unknown. The boundary conditions implied here are vibration at uniformly distributed pressure on a thin flexible disk and zero velocity beyond its rim. The expressions are relatively compact and do not involve numerical integration and thus no difficulties in computation except that there is a singularity at the rim. The Rayleigh integral and Rayleigh's far-field approximation are solved for the near-field and the far-field pressures, respectively. The King integral is solved for the immediate near-field expression.

In the latter article by Mellow [74], the closed form expressions for near-field, immediate near-field, and far-field acoustic pressure distribution for a resilient disk source in free space are derived. The source considered is the simplest dipole planar source where the disk has a uniform pressure across the face and no pressure beyond its rim. It can be used as a model for a flexible membrane or diaphragm in free space. The near-field expression derived is extended for the case where the driving pressure distribution is arbitrary. The relationship between a resilient disk in free space and a rigid

disk in an infinite baffle is also discussed (since they are complementing axisymmetric planar sources).

In 2009, Aarts and Janssen published an article on the on-axis and far-field acoustic pressure expression due to two resilient sources [75]. They worked on resilient flat disk and dome-shaped radiators in an infinite baffle. Utilizing Zernike expansion of azimuthal order 0 to describe the radially symmetric velocity distribution, the series expressions involve Zernike expansion coefficients, and Bessel and Hankel functions. In the inverse problem, the velocity distribution is estimated from on-axis pressure by approximating the Zernike expansion coefficient. A few terms of Zernike expansion are adequate to represent a well-behaved velocity distribution, showing that velocity profiles of resilient radiators are proficiently described by Zernike polynomials.

2.4 Acoustic Microscope

Acoustic microscopy has a fairly short story compared to the probe transducer. The Russian scientist named Sokolov is known to be the father of acoustic microscopy [15, 76, 77]. He was the first person to use acoustic radiation to visualize the internal structure of materials. He conducted an experiment in 1940's, in which he succeeded to obtain high-frequency acoustic images [78]. Due to the limited capability of equipment, at that time, the power of acoustic microscopy was withheld. Advancement of the technology in wave generation and reception enabled the visualization of high-frequency sound in hypersonic range in early 1970's [79, 80].

In the early stage of the development of the Acoustic Microscope, there were two approaches. The first one approach was proposed by Corpel and Kessler [79]. In their

approach, a laser beam has been used to read a pattern formed at the liquid boundary generated by an irradiated specimen immersed in water. The first commercial product based on this principle was built in 1975, and the microscope was able to achieve an image of the order of 20 to 25 μm at a sensitivity of 10 W/cm at 100 MHz operating frequency. However, the resolution of this type of microscope cannot be enhanced due to the underlying principle.

The other approach is the basis of modern acoustic microscopes made possible to obtain high-resolution images. In 1974, Quate and Lemons created the first scanning acoustic microscope [80]. In this method, a focused beam has been used to radiate and scan across a specimen. The acoustic image is, then, formed by the deviation in received signals at different scanning positions. The operating frequency of the microscope determines its resolution in this type of acoustic microscope.

A modern acoustic microscope can determine the size and location of objects inside a solid, thanks to the recent developments in the theory of acoustic microscopy [14, 81, 82]. In 1992, Briggs published a book in which he described many applications of acoustic microscopy, such as inspection of biological tissue, layered structures, and surface cracks. Crossen *et al.* combined acoustic microscopy with time-of-flight technique to investigate adhesion problems [83] while Levin *et al.* studied microstructure of super-hard materials [84]. Moreover, stress inside solid materials can be visualized using acoustic microscopes [85]. The ultrasonic force microscope [86] and the atomic force acoustic microscope [87] pushed the resolution of the conventional acoustic microscope to the nanometer range in recent years.

CHAPTER 3

WAVES

3.1 Wave Propagation through an Infinite Space

Depending on the location of propagation within a medium, mechanical waves can be characterized in to two types: (a) body waves, and (b) guided waves. Body waves are the waves that pass though the interior of a medium, whereas guided waves are the wave that propagates along the boundaries or the interfaces of unbounded media or may also be confined within two boundaries of bounded media. Body waves can be further classified to longitudinal and transverse waves. Rayleigh waves, Love waves, Stonley waves are several examples of the guided wave. In the following section, wave transmission is discussed further.

3.1.1 Body Waves

Body waves are waves that pass through the material. Longitudinal and transverse are the types of the body waves. Longitudinal waves are compressional waves that are longitudinal in nature and the vibration direction is parallel to the direction of wave propagation. They are also called as primary wave or P-wave. Transverse waves are commonly known as Secondary wave, Shear waves or S wave and they propagate in the

transverse direction. The P-wave and S- waves are represented at figure 3.1(a) & (b) respectively. Depending on the perpendicular to the travelling direction, there are two possible direction on which the particle can oscillate. If the oscillation plane is similar to the propagation direction, then it is called vertically polarized shear wave and is denoted by SV. If the oscillation is in and out of plane of the direction of travel, then it is called horizontally polarized shear wave or SH wave.

Body Waves

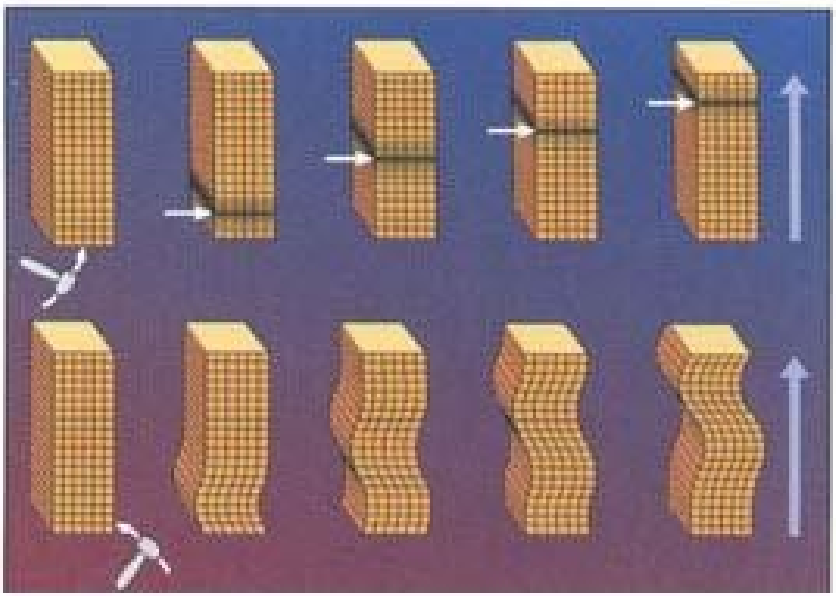

Figure 3.1 Particle movements of body waves [ref. C]

3.1.2 Guided Waves

Guided waves can be of two types: (a) surface wave and (b) interface wave. Surface waves travel on and near the surface and interface waves are limited to an interface. For these waves, the energy dissipation is very rapid with the movement when the waves are away from the surface or interface. Rayleigh wave is a kind of surface

wave that travels like the ripples in motion. The speed of Rayleigh wave is around 90% of the shear wave speed in any given medium, and it can penetrate roughly 1.5 times the wavelength beneath the surface of a medium. Love waves are another kind of surface waves which can propagate through a layered solid half space that is an infinite medium bounded by one surface. Particle movement direction is the main difference between Rayleigh wave and Love wave. In Rayleigh wave, the particle motion forms an ellipse in the same plane as direction of propagation. The particle motion of Love wave is in the direction perpendicular to the direction of propagation. The movements of the particles are illustrated in figure 3.2 (a) and (b).

The propagation of Lamb wave in a plate or a structure needs to have much smaller thickness than the other two dimensions with the stress-free boundaries on the plate surfaces. Cylindrical guided waves are the waves that propagate through a rod- or pipe-like structure.

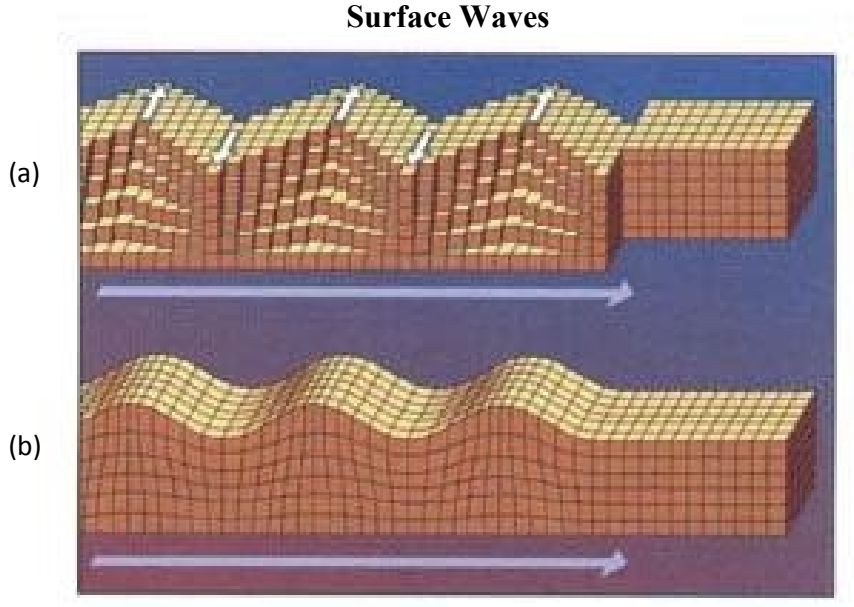

Figure 3.2 Particle movements of surface waves [ref. C]

3.2 Wave Equation

3.2.1 Equation of Motion

For a homogeneous isotropic elastic body, the equation of motion can be written in tensor or index notation as

$$\sigma_{ij,j} + f_i = \rho\ddot{u} \tag{3 - 1}$$

where, σ_{ij} is the stress tensor at a point, and f_i and u_i are the body force and displacement vectors, respectively. P is the mass density per unit volume of the body.

The constitutive relationship for linear isotropic material is given by

$$\sigma_{ij} = 2\mu\varepsilon_{ij} + \lambda\varepsilon_{kk}\delta_{ij} \tag{3 - 2}$$

The strain and rotation tensors are defined as follows:

$$\varepsilon_{ij} = \frac{1}{2}\left(u_{i,j} + u_{j,i}\right) \tag{3 - 3}$$

$$\omega_{ij} = \frac{1}{2}\left(u_{i,j} - u_{j,i}\right) \tag{3 - 4}$$

where, ε_{ij} and ω_{ij} are the strain and rotation tensors, respectively. The constants μ and λ are the elastic constants known as the Lamé constants. The relationship between the stress tensor and displacement can be obtained by substituting equation 3-2 and 3-3 into equation 3-1, and the so called Navier's equation is obtained.

$$(\lambda + \mu)u_{j,ji} + \mu u_{i,jj} + f_i = \rho\ddot{u}_i \tag{3 - 5}$$

In vector form, the equation is written as,

$$(\lambda + \mu)\underline{\nabla}\left(\underline{\nabla}.\mathrm{u}\right) + \mu\nabla^2\mathrm{u} + \mathrm{f} = \rho\ddot{\mathrm{u}} \tag{3 - 6}$$

Using the vector identity, $\nabla^2\mathbf{u} = \underline{\nabla}\left(\underline{\nabla}.\mathbf{u}\right) - \underline{\nabla} \times \underline{\nabla} \times \mathbf{u}$, one can write equation 3-6 as

$$(\lambda + \mu)\underline{\nabla}\left(\underline{\nabla}.\mathbf{u}\right) - \mu\underline{\nabla} \times \underline{\nabla} \times \mathbf{u} + \mathbf{f} = \rho\ddot{\mathbf{u}} \tag{3 - 7}$$

In index notations, equations 3-6 and 3-7 can be expressed as

$$(\lambda + \mu)u_{j,ij} + \mu u_{i,jj} + f_i = \rho\ddot{u}_i \tag{3 - 8}$$

And

$$(\lambda + 2\mu)u_{j,ij} + \mu\varepsilon_{ijk}\varepsilon_{kmn}u_{n,mj} + f_i = \rho\ddot{u}_i \tag{3 - 9}$$

respectively. ε_{ijk} and ε_{kmn} are permutation symbols.

Equations 3-7, 3-8, and 3-9 subjected to proper boundary conditions give rise to various elastic waves. However, there is no general solution for two- or three-dimensional Navier's equation. It is common practice to apply Stokes-Helmholtz decomposition to transform Navier's equation into wave equations.

3.2.2 Helmholtz Decomposition

Helmholtz's theorem states that any sufficiently smooth, rapidly decaying vector field in three dimensions can be resolved into the sum of an irrotational vector field and a solenoidal vector field. This indicates that a pair of potentials—a scalar potential and a

vector potential, can generate such vector field. Applying this theorem, any displacement field **u** can be decomposed as

$$\mathbf{u} = \underline{\nabla}\emptyset + \underline{\nabla} \times \mathbf{A} \tag{3 - 10}$$

where ϕ is a scalar potential, and **A** is a vector potential. In order to ensure unique relation between the components of **u** (u_1 , u_2 , and u_3) and ϕ, A_1 , A_2 , A_3 , the following auxiliary condition is defined:

$$\underline{\nabla}.\mathbf{A} = 0 \tag{3 - 11}$$

Substituting Equation 2-10 in the absence of a body force, Equation 2-6 can be written as

$$(\lambda + \mu)\underline{\nabla}\left[\underline{\nabla}.\left(\underline{\nabla}\emptyset + \underline{\nabla} \times \mathbf{A}\right)\right] - \mu\underline{\nabla} \times \underline{\nabla} \times \left(\underline{\nabla}\emptyset + \underline{\nabla} \times \mathbf{A}\right) + \mathbf{f} = \rho\left(\underline{\nabla}\ddot{\emptyset} + \underline{\nabla} \times \ddot{\mathbf{A}}\right) \tag{3 - 12}$$

Using the auxiliary condition (Equation 2-11), Equation 2-12 can be simplified to

$$\begin{aligned} &(\lambda + 2\mu)\underline{\nabla}(\nabla^2\emptyset) - \mu\underline{\nabla} \times (-\nabla^2\mathbf{A}) = \rho\left(\underline{\nabla}\ddot{\emptyset} + \underline{\nabla} \times \ddot{\mathbf{A}}\right) \\ &\underline{\nabla}\left[(\lambda + 2\mu)\nabla^2\emptyset - \rho\ddot{\emptyset}\right] + \underline{\nabla} \times \left(\mu\nabla^2\mathbf{A} - \rho\ddot{\mathbf{A}}\right) = 0 \end{aligned} \tag{3 - 13}$$

Note that, the following vector identities are used to obtain equation 3-13:

$$\begin{aligned} &\underline{\nabla}.\left(\underline{\nabla} \times \mathbf{A}\right) = 0 \\ &\underline{\nabla} \times \left(\underline{\nabla}\emptyset\right) = 0 \\ &\underline{\nabla} \times \underline{\nabla} \times \mathbf{A} = \underline{\nabla}\left(\underline{\nabla}.\mathbf{A}\right) - \nabla^2\mathbf{A} \end{aligned} \tag{3 - 14}$$

The following conditions are sufficient to satisfy equation 3-13:

$$(\lambda + 2\mu)\nabla^2\emptyset - \rho\ddot{\emptyset} = 0$$

$$\mu\nabla^2\mathbf{A} - \rho\ddot{\mathbf{A}} = 0$$

3.2.3 One-Dimensional Wave Equation

Dividing both sides of the above equations by the coefficients of the first terms, the above equations can be written as:

$$\nabla^2\emptyset - \frac{\rho}{(\lambda + 2\mu)}\ddot{\emptyset} = \nabla^2\emptyset - \frac{1}{c_p^2}\ddot{\emptyset} = 0$$

$$\nabla^2\mathbf{A} - \frac{\rho}{\mu}\ddot{\mathbf{A}} = \nabla^2\mathbf{A} - \frac{1}{c_s^2}\ddot{\mathbf{A}} = 0 \qquad (3 - 15)$$

where,

$$c_p = \sqrt{\frac{(\lambda+2\mu)}{\rho}}$$

$$c_s = \sqrt{\frac{\mu}{\rho}}$$

Both equations in Equation 3-15 are one-dimensional wave equation. It can be shown that Equation 3-15 has a solution in the form of

$$\emptyset(\mathbf{x}, t) = \emptyset\big(\mathbf{n}.\mathbf{x} - c_p t\big)$$

$$A(\mathbf{x}, t) = A(\mathbf{n}.\mathbf{x} - c_s t) \qquad (3 - 16)$$

These equations correspond to the waves travelling in the n direction with the velocity c_p and c_s, respectively. n is an arbitrary unit vector.

From equation 3-10 and 3-16, the displacement field u can be written as

$$\mathbf{u} = \underline{\nabla}\emptyset\big(\mathbf{n}.\mathbf{x} - c_p t\big) + \underline{\nabla} \times \mathbf{A}(\mathbf{n}.\mathbf{x} - c_s t)$$

$$= \mathbf{n}\emptyset'\big(\mathbf{n}.\mathbf{x} - c_p t\big) + \underline{\nabla} \times \mathbf{A}(\mathbf{n}.\mathbf{x} - c_s t)$$

where, $\emptyset'$ is the derivative of $\emptyset$ with respect to its argument.

When A=0, the displacement expression simplifies to

$$\mathbf{u} = \mathbf{n}\emptyset'(\mathbf{n}.\mathbf{x} - c_p t) \tag{3 - 17}$$

Note that the displacement vector is in the same direction as the propagating wave; therefore, the displacement field in Equation 3-17 corresponds to longitudinal waves or P-waves by definition.

On the other hand, if $\emptyset = 0$, the displacement expression becomes

$$\mathbf{u} = \underline{\nabla} \times \mathbf{A}(\mathbf{n}.\mathbf{x} - c_s t) \tag{3 - 18}$$

This can be written in terms of components in the Cartesian coordinate as

$$u_1 = n_2 A_3'(\mathbf{n}.\mathbf{x} - c_s t) - n_3 A_2'(\mathbf{n}.\mathbf{x} - c_s t)$$

$$u_2 = n_3 A_1'(\mathbf{n}.\mathbf{x} - c_s t) - n_1 A_3'(\mathbf{n}.\mathbf{x} - c_s t)$$

$$u_3 = n_1 A_2'(\mathbf{n}.\mathbf{x} - c_s t) - n_2 A_1'(\mathbf{n}.\mathbf{x} - c_s t)$$

Then, the dot product between n and u becomes

$$\begin{aligned} n.u = {} & n_1[n_2 A_3'(\mathbf{n}.\mathbf{x} - c_s t) - n_3 A_2'(\mathbf{n}.\mathbf{x} - c_s t)] \\ & + n_2[n_3 A_1'(\mathbf{n}.\mathbf{x} - c_s t) - n_1 A_3'(\mathbf{n}.\mathbf{x} - c_s t)] \\ & + n_3[n_1 A_2'(\mathbf{n}.\mathbf{x} - c_s t) - n_2 A_1'(\mathbf{n}.\mathbf{x} - c_s t)] = 0 \end{aligned}$$

Thus the displacement vector u is perpendicular to the direction of propagation, n, and equation 3-18 corresponds to the shear wave or S- wave.

CHAPTER 4

DISTRIBUTED POINT SOURCE METHOD

4.1 Principle of DPSM

The main principal on which DPSM is based is the Huygens' Principle. In Huygens' Principal, it is stated that, in a wave front, every point may be considered as the source of secondary wavelets that spreads out in all the directions with identical speed as the propagating wave. If a point emits a spherical wave depicted in Figure 4.1 (a) and multiple point sources are placed in a line shown in (b), then the wave front of such points form a cylindrical shape shown in (c) provided that sufficient number of points are positioned next to each other since the neighboring points cancel the opposing wave fronts. Although it is not shown in the figure, the same principle can be easily extended to two-dimensional space to represent a planar radiation source. Huygens' Principle also enables to relate the speed of a propagating wave some distance away from the source to that at the point of emission. Thus, given the speed of a wave at a certain location, the speed at any point can be determined.

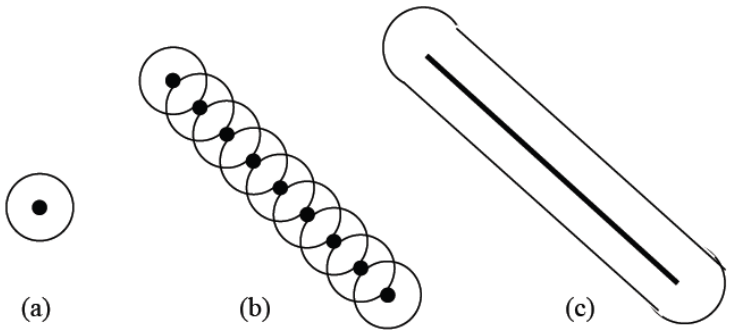

Figure 4.1 Huygens' Principle

For example, let us consider an ultrasonic transducer immersed in a fluid medium. Let, for this problem, G(x,y) be the Green's function for the equation of motion. If the excitation of the transducer is represented by N points of amplitudes A_m, then the solution at point **x** can be expressed as

$$u(\mathbf{x}) = \sum_{m=1}^{N} A_m G(\mathbf{x_m}, \mathbf{y_m}) \tag{4- 1}$$

This is illustrated in Figure 4.2. When solutions at M target points are sought, the equation forms the system of M equations shown in Equation 4-2.

$$\begin{Bmatrix} u(\mathbf{x_1}) \\ u(\mathbf{x_2}) \\ \vdots \\ u(\mathbf{x_M}) \end{Bmatrix} = \begin{bmatrix} G(\mathbf{x}_1, \mathbf{y}_1) & G(\mathbf{x_1}, \mathbf{y}_2) & \cdots & G(\mathbf{x_1}, \mathbf{y}_N) \\ & & & \vdots \\ & & & \vdots \\ & & & G(\mathbf{x_M}, \mathbf{y}_N) \end{bmatrix} \begin{Bmatrix} A_1 \\ A_2 \\ \vdots \\ A_N \end{Bmatrix} \tag{4- 2}$$

or **u** = **D**$\underline{\mathbf{A}}$. Applying the boundary condition of the transducer surface, this system of equations can be solved for the amplitudes at the same location by inverting the matrix **D** as

$$\mathbf{A} = \underline{\mathbf{D^{-1}}}\mathbf{u} \tag{4-3}$$

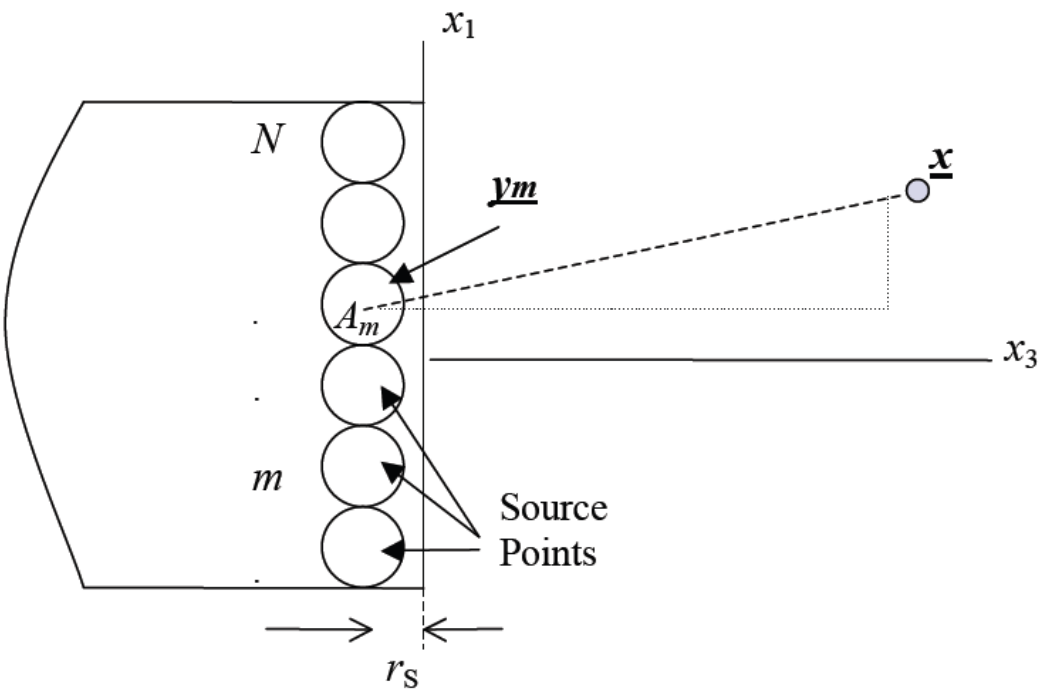

Figure 4.2 Point sources representing a transducer

4.2 Comparison of DPSM to Other Numerical Methods

The immediate benefit of modeling with DPSM is that it can handle a complex geometry like the Finite Element Method (FEM) but point sources are distributed only at the surface of a structure unlike in FEM [27, 88]. This significantly decreases the size of the matrices involved in the computations as complexity and size of the structure increase. In addition, DPSM yields the solution with accuracy better than that of FEM for ultrasonic applications. Since DPSM does not require full-space discretization as FEM does, it conserves the computation time and space. It becomes exceedingly propitious when wave

frequency increases because size of an element in FEM must decrease at high frequencies. In addition, DPSM is more accurate when accounting for an infinite boundary condition in the calculation. Since the FEM must introduce a finite boundary in modeling, it imitates infinite boundaries by assigning extra layers of elements with damping properties to absorb the wave to eliminate the reflection from the boundaries. However this adds the extra elements on top of the already computationally expensive method.

4.3 Pressure and Displacement Green's Functions in Fluid

The equation of motion is given by

$$\sigma_{ij},j + f_i = \rho\ddot{u}_\iota \tag{4- 3}$$

In order to obtain the fundamental solution for a fluid medium, the fluid is assumed to be a perfect fluid. Perfect fluids have no shear stresses, viscosity, or heat conduction. The constitutive relation for isotropic materials can be specialized for perfect fluids by setting $\mu = 0$.

$$\sigma_{ij} = 2\mu\varepsilon_{ij} + \lambda\varepsilon_{kk}\delta_{ij} = \lambda\varepsilon_{kk}\delta_{ij} \tag{4- 4}$$

Since hydrostatic pressure *p* is the only stress in a fluid, the stress field is given by:

$$\sigma_{11} = \sigma_{22} = \sigma_{33} = -p$$

Then Equation 4-4 can be written as

$$-p = \sigma_{11} = \sigma_{22} = \sigma_{33}$$

$$= \lambda(\varepsilon_{11} + \varepsilon_{22} + \varepsilon_{33})$$

$$= \lambda\left(u_{1,1} + u_{2,2} + u_{3,3}\right)$$

$$= \lambda \underline{\nabla}.\,\mathbf{u}$$

Or

$$-\frac{p}{\lambda} = \underline{\nabla}.\,\mathbf{u} \tag{4- 5}$$

Since there is no shear stress, the equation of motion (Equation 4-3) can be simplified to

$$\begin{cases} \sigma_{11,1} + f_1 = \rho\ddot{u}_1 \\ \sigma_{22,2} + f_2 = \rho\ddot{u}_2 \\ \sigma_{33,3} + f_3 = \rho\ddot{u}_3 \end{cases} \Longrightarrow \begin{cases} -p_{,1} + f_1 = \rho\ddot{u}_1 \\ -p_{,2} + f_2 = \rho\ddot{u}_2 \\ -p_{,3} + f_3 = \rho\ddot{u}_3 \end{cases}$$

Or simply,

$$-\underline{\nabla}p + \mathbf{f} = \rho\ddot{\mathbf{u}} \tag{4- 6}$$

Taking the divergence on both sides of Equation 4-6 gives

$$\underline{\nabla}.\left(-\underline{\nabla}p + \mathbf{f}\right) = \underline{\nabla}.\,(\rho\ddot{\mathbf{u}})$$

$$-\underline{\nabla}.\,\underline{\nabla}p + \underline{\nabla}.\,\mathbf{f} = \rho\underline{\nabla}.\,\ddot{\mathbf{u}}$$

$$-\underline{\nabla^2}p + \underline{\nabla}.\,\mathbf{f} = \rho\underline{\nabla}.\frac{\delta^2\mathbf{u}}{\delta t^2}$$

Exchanging the order of the divergence operator and time derivative and letting $f = \underline{\nabla}.\,\mathbf{f}$ produces

$$-\nabla^2 p + f = \rho \frac{\partial}{\partial t}(\underline{\nabla}.\mathbf{u})$$

Substituting Equation 4-5 into the above equation gives

$$-\nabla^2 p + f = \rho \frac{\partial^2}{\partial t^2}\left(-\frac{p}{\lambda}\right)$$

$$-\nabla^2 p + f = -\frac{\rho}{\lambda}\frac{\partial^2 p}{\partial t^2}$$

$$\nabla^2 p - \frac{\rho}{\lambda}\frac{\partial^2 p}{\partial t^2} = f$$

$$\nabla^2 p - \frac{1}{c_f^2}\frac{\partial^2 p}{\partial t^2} = f \qquad (4\text{- }7)$$

Where, $c_f = \sqrt{\frac{\lambda}{\rho}}$

Equation 4-8 is the wave equation for a fluid medium.

4.3.1 Point Source in Fluid

A point source in a fluid medium can be considered a radially oscillating sphere whose size is infinitesimally small. In an unbounded fluid, the wave generated is called a spherical (bulk) wave, named after the shape of its wave front. When a point source is generating the wave, its force contributes to the body force term in the wave equation; thus,

$$\nabla^2 p - \frac{1}{c_f^2}\frac{\partial^2 p}{\partial t^2} = f(t)\delta(\mathbf{x}-\mathbf{y}) \tag{4- 8}$$

Where $\delta(x-y)$ is the Dirac delta function whose properties are as follows:

$$\delta(\mathbf{x}-\mathbf{y}) = 0 \qquad \mathbf{x} \neq \mathbf{y}$$

$$\int_V h(\mathbf{y})\delta(\mathbf{x}-\mathbf{y})dV(\mathbf{y}) = \begin{cases} h(x) & \mathbf{x}\ inside\ V \\ \frac{1}{2}h(\mathbf{x}) & \mathbf{x}\ on\ S \\ 0 & \mathbf{x}\ outside\ V \end{cases}$$

Since the pressure disturbance produced by a point source should only be the function of radial distance from the point source, it is convenient to rewrite Equation 4-9 in spherical

$$\nabla^2 = \frac{1}{r}\left[\frac{\partial}{\partial r}\left(r^2\frac{\partial}{\partial r}\right)\right]$$

Then, for $x \neq y$, the wave equation becomes

$$\frac{1}{r^2}\left[\frac{\partial}{\partial r}\left(r^2\frac{\partial p}{\partial r}\right)\right] - \frac{1}{c_f^2}\frac{\partial^2 p}{\partial t^2} = 0$$

Without the loss of generality, we can assume $p = P(r,t)/r$. Then,

$$\frac{1}{r^2}\left\{\frac{\partial}{\partial r}\left[r^2\frac{\partial}{\partial r}\left(\frac{P}{r}\right)\right]\right\} - \frac{1}{c_f^2}\frac{\partial^2}{\partial t^2}\left(\frac{P}{r}\right) = 0$$

$$\frac{1}{r^2}\left\{\frac{\partial}{\partial r}\left[r^2\left(\frac{1}{r}\frac{\partial P}{\partial r} - P\frac{1}{r^2}\right)\right]\right\} - \frac{1}{rc_f^2}\frac{\partial^2 P}{\partial t^2} = 0$$

$$\frac{1}{r^2}\left\{\frac{\partial}{\partial r}\left[\left(r\frac{\partial P}{\partial r} - P\right)\right]\right\} - \frac{1}{rc_f^2}\frac{\partial^2 P}{\partial t^2} = 0$$

$$\frac{1}{r^2}\left(\frac{\partial P}{\partial r}+r\frac{\partial^2 P}{\partial r^2}-\frac{\partial P}{\partial r}\right)-\frac{1}{rc_f^2}\frac{\partial^2 P}{\partial t^2}=0$$

$$\frac{\partial^2 P}{\partial r^2}-\frac{1}{c_f^2}\frac{\partial^2 P}{\partial t^2}=0 \tag{4- 9}$$

Equation 4-10 is simply the wave equation in one-dimension, *r*, and it can be shown that the equation has general solutions of the form:

$$P=P_1\left(t-\frac{r}{c_f}\right)+P_2\left(t+\frac{r}{c_f}\right)$$

where P_1 and P_2 are arbitrary functions. The function P_1 corresponds to a wave traveling in the $+r$ direction (outward), and P_2 corresponds to a wave traveling in the $-r$ (inward) direction. Physically, it is impossible for a point source to have an inwardly propagating wave; therefore, the solution should be of the form:

$$p=\frac{P}{r}=\frac{1}{r}P_1\left(t-\frac{r}{c_f}\right)$$

It can be shown that the relationship between the temporal part of P_1 and force *f(t)* in the wave equation is $-4\pi P_1(t)=-f(t)$ [89]. Thus, the pressure expression becomes

$$p=\frac{1}{4\pi r}f\left(t-\frac{r}{c_f}\right)$$

If a point source emits an impulsive force, the time function *f* itself is a delta function. The governing wave equation and its solution, then, can be expressed as

$$\nabla^2 p - \frac{1}{c_f^2}\frac{\partial^2 p}{\partial t^2} = \delta(t)\delta(\mathbf{x}-\mathbf{y}) \tag{4- 10}$$

$$p(r,t) = \frac{1}{4\pi r}\delta\left(t - \frac{r}{c_f}\right) \tag{4- 11}$$

Taking the Fourier transforms of equations 4-11 and 4-12 gives

$$\nabla^2 G - \frac{\omega^2}{c_f^2}\frac{\partial^2 G}{\partial t^2} = \exp(-i\omega t)\delta(\mathbf{x}-\mathbf{y})$$

$$G(r,\omega) = \frac{exp\left(\frac{i\omega r}{c_f}\right)}{4\pi r} = \frac{exp(ik_f r)}{4\pi r}$$

Where G is the Fourier transform of *p*. Note that G is also the solution for harmonically excited point sources in the fluid.

4.3.2 Displacement Field in Fluid

Using Helmholtz decomposition, any displacement field **u** due to a point source in fluid can be written in terms of a scalar potential φ and a vector potential **A** as $\mathbf{u} = \underline{\nabla}\varphi + \underline{\nabla} \times \mathbf{A}$. The displacement corresponding to $\underline{\nabla}\varphi$ represents the P-wave and generates normal stresses in the medium while the displacement corresponding to $\underline{\nabla} \times \mathbf{A}$ represents the S-wave and generates shear stresses in the medium. Since there should be no shear stress in ideal fluid, the displacement is expressed as

$$\mathbf{u} = \underline{\nabla}\varphi \tag{4- 12}$$

For harmonic time dependency, the potential φ takes the following form

$$\varphi(\underline{x}, t) = \varphi(\mathbf{n}.\mathbf{x} - c_f t)$$

$$= B \exp(ik_f \mathbf{x} - i\omega t)$$

Without loss of generality, one can let B=1. When the harmonic time dependency is implied, from equation 4-6, the pressure-potential relation can be obtained as

$$-\frac{p}{\lambda} = \underline{\nabla}.\mathbf{u}$$

$$= u_{1,1} + u_{2,2} + u_{3,3}$$

$$= \frac{\partial^2 \varphi}{\partial x_1^2} + \frac{\partial^2 \varphi}{\partial x_2^2} + \frac{\partial^2 \varphi}{\partial x_3^2}$$

$$= \nabla^2 \varphi$$

$$= -k_f^2 \exp(ik_f x)$$

$$= -k_f^2 \varphi$$

Or

$$\varphi = -\frac{p}{\lambda k_f^2} = -\frac{c_f^2 p}{\lambda \omega^2} = -\frac{p}{\rho \omega^2}$$

In terms of Green's function, the potential can be expressed as

$$\varphi = -\frac{\exp(ik_f r)}{4\pi\rho\omega^2 r}$$

Therefore, the displacements in fluid are given in spherical coordinates by

$$\mathbf{u}(r) = \frac{1}{4\pi\rho\omega^2 r} k_f^2 \exp(ik_f r) \tag{4- 13}$$

In Cartesian coordinates, the displacements due to a point source in all three directions are written as

$$u_1 = \frac{1}{4\pi\rho\omega^2}\left[\frac{1}{r} ik_f R_1 \exp\left(ik_f r\right) - \frac{\exp\left(ik_f r\right)}{r^2} R_1\right] \tag{4- 14}$$

$$u_2 = \frac{1}{4\pi\rho\omega^2}\left[\frac{1}{r} ik_f R_2 \exp\left(ik_f r\right) - \frac{\exp\left(ik_f r\right)}{r^2} R_2\right] \tag{4- 15}$$

$$u_3 = \frac{1}{4\pi\rho\omega^2}\left[\frac{1}{r} ik_f R_3 \exp\left(ik_f r\right) - \frac{\exp\left(ik_f r\right)}{r^2} R_3\right] \tag{4- 16}$$

where $R_i = \frac{x_i - y_i}{r}$

4.4 Pressure and Velocity Fields in Fluids Due to Multiple Point Sources

Placing a substantial number of point sources can model the wave generated by a finite planar surface. When point sources are distributed over a surface, the pressure field at position **x** due to the sources at position **y** can be determined by integrating the individual contributions over the surface. Therefore, the pressure field can be given by

$$p(\mathbf{x}) = \int_S B \frac{\exp\left(ik_f r\right)}{4\pi r} dS(\mathbf{y}) \tag{4- 17}$$

where B is the strength of the point sources. Equation 4-18 can be written in the summation form as:

$$p(\mathbf{x}) = \sum_{m=1}^{N} \left(\frac{B}{4\pi}\Delta S_m\right)\frac{\exp(ik_f r_m)}{r_m} = \sum_{m=1}^{N} A_m \frac{\exp(ik_f r_m)}{r_m} \tag{4- 18}$$

where N is the number of point sources distributed over the surface S. The subscript m indicates m-th point source. S_m is the elemental surface area, A_m is the source strength, and r_m is the distance from the m-th point source to a target point **x**.

4.4.1 Pressure-Velocity Relation

In the absence of a body force, the equation of motion in a fluid medium can be written as

$$-\underline{\nabla} p = \rho \ddot{\mathbf{u}}$$

$$-\underline{\nabla} p = \rho \dot{v} = \rho \frac{\partial v}{\partial t}$$

Taking the dot product on both sides of the above equation with a unit vector **n** gives

$$-\underline{\nabla} p.\mathbf{n} = \rho \frac{\partial (v.\mathbf{n})}{\partial t} \tag{4- 19}$$

The left hand side of the above equation can be written as

$$-\underline{\nabla} p.\mathbf{n} = -\frac{\partial p}{\partial x_i}\frac{\partial x_i}{\partial n} = -\frac{\partial \rho}{\partial n}$$

The right hand side of Equation 4-20 can be simplified to

$$\rho \frac{\partial (\mathbf{v}.\mathbf{n})}{\partial t} = \rho \frac{\partial v_n}{\partial t}$$

Therefore, Equation 4-20 can also be expressed in the following form,

$$-\frac{\partial p}{\partial n} = \rho \frac{\partial v_n}{\partial t} \tag{4- 20}$$

Integrating both sides leads to

$$v_n = -\int \frac{1}{\rho} \frac{\partial p}{\partial n} dt \tag{4- 21}$$

For harmonic time dependency with constant material properties,

$$\begin{aligned} v_n &= -\frac{1}{\rho} \frac{\partial p(\mathbf{x})}{\partial n} \int e^{-i\omega t} dt \\ &= \frac{1}{i\omega\rho} \frac{\partial p(\mathbf{x})}{\partial n} e^{-i\omega t} \end{aligned} \tag{4- 22}$$

Thus, using the pressure expression in Equation 4-19, the velocity due to the *m*-th point source can be obtained (harmonic time dependency is implied)

$$\begin{aligned} v_m(r) &= \frac{A_m}{i\omega\rho} \frac{\partial}{\partial r} \left(\frac{\exp(ik_f r)}{r} \right) \\ &= \frac{A_m}{i\omega\rho} \left(\frac{ik_f \exp(ik_f r)}{r} - \frac{\exp(ik_f r)}{r^2} \right) \\ &= \frac{A_m}{i\omega\rho} \frac{\exp(ik_f r)}{r} \left(ik_f - \frac{1}{k_f} \right) \end{aligned} \tag{4- 23}$$

Then, the velocity components in all three directions due to *m*-th point source are

$$v_{1m}(r) = \frac{A_m}{i\omega\rho} \frac{\partial}{\partial x_1} \left(\frac{\exp(ik_f r)}{r} \right) = \frac{A_m}{i\omega\rho} \frac{x_1 \exp(ik_f r)}{r^2} \left(ik_f - \frac{1}{r} \right) \tag{4- 24}$$

$$v_{2m}(r) = \frac{A_m}{i\omega\rho}\frac{\partial}{\partial x_2}\left(\frac{\exp(ik_f r)}{r}\right) = \frac{A_m}{i\omega\rho}\frac{x_2\exp(ik_f r)}{r^2}\left(ik_f - \frac{1}{r}\right) \quad (4\text{- }25)$$

$$v_{3m}(r) = \frac{A_m}{i\omega\rho}\frac{\partial}{\partial x_3}\left(\frac{\exp(ik_f r)}{r}\right) = \frac{A_m}{i\omega\rho}\frac{x_3\exp(ik_f r)}{r^2}\left(ik_f - \frac{1}{r}\right) \quad (4\text{- }26)$$

Where $r = \sqrt{x_1^2 + x_2^2 + x_3^2}$

The total velocity at target point $\underline{x}$ due to N number of point sources can be obtained simply by adding the contributions from all N point sources. Thus,

$$v_1(x) = \sum_{m=1}^{N} v_{1m}(r_m) = \sum_{m=1}^{N} \frac{A_m}{i\omega\rho}\frac{x_{1m}\exp(ik_f r_m)}{r_m^2}\left(ik_f - \frac{1}{r_m}\right) \quad (4\text{- }27)$$

$$v_2(x) = \sum_{m=1}^{N} v_{2m}(r_m) = \sum_{m=1}^{N} \frac{A_m}{i\omega\rho}\frac{x_{2m}\exp(ik_f r_m)}{r_m^2}\left(ik_f - \frac{1}{r_m}\right) \quad (4\text{- }28)$$

$$v_3(x) = \sum_{m=1}^{N} v_{3m}(r_m) = \sum_{m=1}^{N} \frac{A_m}{i\omega\rho}\frac{x_{3m}\exp(ik_f r_m)}{r_m^2}\left(ik_f - \frac{1}{r_m}\right) \quad (4\text{- }29)$$

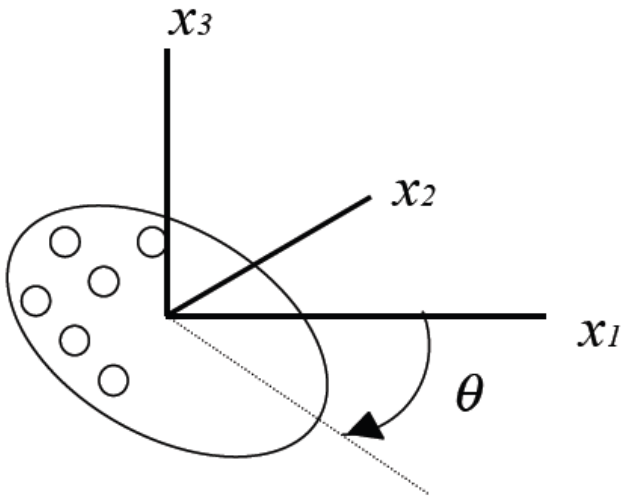

Figure 4.3 Rotation of the radiation source by θ about axis x_2

If the surface represented by the point sources is inclined at an angle θ as shown in Figure 4.3, the velocity component normal to the inclined surface can be easily determined by

$$v_n(x) = v_1(x)\sin\theta + v_3(x)\cos\theta$$

$$= \sum_{m=1}^{N} \frac{A_m}{i\omega\rho}\left(ik_f - \frac{1}{r_m}\right)\left[\frac{x_{1m}\exp(ik_f r_m)}{r_m^2} sin\theta + \frac{x_{3m}\exp(ik_f r_m)}{r_m^2} cos\theta\right] \qquad (4\text{-}30)$$

Note that the rotation is by angle θ about the x_2 -axis and that the x_3 -axis is no longer aligns with the outward normal of the surface.

4.4.2 Matrix Representation

The velocity at M target or observation points due to N source points forms a $M \times 1$ vector.

$$\mathbf{V} = [\mathbf{v}^1 \quad \mathbf{v}^2 \quad \mathbf{v}^3 \quad \cdots \quad \cdots \quad \cdots \quad \mathbf{v}^{M-1} \quad \mathbf{v}^M]^T$$

where $\mathbf{v}^n$ is the velocity at the n-th target point.

When the strength of N source points varies, the source strength can be expressed as a $N \times 1$ vector

$$\mathbf{A} = [\mathbf{A}_1 \quad \mathbf{A}_2 \quad \mathbf{A}_3 \quad \cdots \quad \cdots \quad \cdots \quad \mathbf{A}_{N-1} \quad \mathbf{A}_N]^T$$

From Equations 4-27 to 4-29, the velocity vector can be related to the source strength vector by

$$\mathbf{V} = \mathbf{MA} \tag{4- 31}$$

The dimensions of **M** matrix are $M \times N$, and it can be written as

$$\mathbf{M} = \begin{bmatrix} f(x_{t1}^1, r_1^1) & f(x_{t1}^2, r_1^2) & f(x_{t1}^3, r_1^3) & \dots & \dots & f(x_{t1}^{N-1}, r_1^{N-1}) & f(x_{t1}^N, r_1^N) \\ f(x_{t2}^1, r_2^1) & f(x_{t2}^2, r_2^2) & f(x_{t2}^3, r_2^3) & \dots & \dots & f(x_{t2}^{N-1}, r_2^{N-1}) & f(x_{t2}^N, r_2^N) \\ f(x_{t3}^1, r_3^1) & f(x_{t3}^2, r_3^2) & \dots & \dots & \dots & \dots & \dots \\ \dots & \dots & \dots & \dots & \dots & \dots & \dots \\ \dots & \dots & \dots & \dots & \dots & \dots & \dots \\ \dots & \dots & \dots & \dots & \dots & \dots & \dots \\ f(x_{tM}^1, r_M^1) & f(x_{tM}^2, r_M^2) & f(x_{tM}^3, r_M^3) & \dots & \dots & f(x_{tM}^{N-1}, r_M^{N-1}) & f(x_{tM}^N, r_M^N) \end{bmatrix}_{M \times N}$$

(4- 32)

Where

$$f(x_m^m, r_n^m) = \frac{x_m^m \exp(ik_f r_n^m)}{i\omega\rho(r_n^m)^2}\left(ik_f - \frac{1}{r_n^m}\right) \tag{4- 33}$$

r_n^m is the distance between *m*-th point source and the *n*-th target point.x_n^m is the distance from *m*-th point source to *n*-th target point along the x_t -axis.

Similarly, using Equation 4-19, the pressure at *M* target points due to *N* source points can be related via

$$\mathbf{Pr} = \mathbf{QA} \tag{4- 34}$$

Where $\mathbf{Pr} = [p^1 \quad p^2 \quad p^3 \quad \dots \quad p^{M-2} \quad p^{M-1} \quad p^M]^T$

The expression for Q is as follows:

$$\mathbf{Q} = \begin{bmatrix} g(r_1^1) & g(r_1^2) & g(r_1^3) & \dots & \dots & g(r_1^{N-1}) & g(r_1^N) \\ g(r_2^1) & g(r_2^2) & g(r_2^3) & \dots & \dots & \dots & \dots \\ g(r_3^1) & g(r_3^2) & \dots & \dots & \dots & \dots & \dots \\ \dots & \dots & \dots & \dots & \dots & \dots & \dots \\ \dots & \dots & \dots & \dots & \dots & \dots & \dots \\ \dots & \dots & \dots & \dots & \dots & \dots & \dots \\ g(r_M^1) & g(r_M^2) & g(r_M^3) & \dots & \dots & g(r_M^{N-1}) & g(r_M^N) \end{bmatrix}_{M\times N} \tag{4- 35}$$

and $$g(r_n^m) = \frac{\exp(ik_f r_n^m)}{r_n^m}$$

In the similar manner, the matrix representation of the displacement components at *M* target points due to *N* number of source points can be found using Equations 4-15, 4-16, and 4-17 as

$$\mathbf{u1} = [\mathbf{DF_1}]\mathbf{A} \tag{4- 36}$$

$$\mathbf{u2} = [\mathbf{DF_2}]\mathbf{A} \tag{4- 37}$$

$$\mathbf{u3} = [\mathbf{DF_3}]\mathbf{A} \tag{4- 38}$$

where,

$$[\mathbf{DFi}] = \begin{bmatrix} h({}^1R_i^1, r_1^1) & h({}^1R_i^2, r_1^2) & h({}^1R_i^3, r_1^3) & \dots & h({}^1R_i^{N-1}, r_1^{N-1}) & h({}^1R_i^N, r_1^N) \\ h({}^2R_i^1, r_2^1) & h({}^2R_i^2, r_2^2) & h({}^2R_i^3, r_2^3) & \dots & h({}^1R_i^{N-1}, r_2^{N-1}) & h({}^1R_i^N, r_2^N) \\ h({}^3R_i^1, r_3^1) & h({}^3R_i^2, r_3^2) & h({}^3R_i^3, r_3^3) & \dots & \dots & \dots \\ h({}^4R_i^1, r_4^1) & h({}^4R_i^2, r_4^2) & \dots & \dots & \dots & \dots \\ \dots & \dots & \dots & \dots & \dots & \dots \\ h({}^MR_i^1, r_M^1) & h({}^MR_i^2, r_M^2) & h({}^MR_i^3, r_M^3) & \dots & h({}^MR_i^{N-1}, r_M^{N-1}) & h({}^MR_i^N, r_M^N) \end{bmatrix} \tag{4- 39}$$

$$h({}^nR_i^m, r_n^m) = \frac{1}{\rho\omega^2}\left[\frac{1}{r} ik_f {}^nR_i^m \exp\left(ik_f r_n^m\right) - \frac{\exp(ik_f r_n^m)}{(r_n^m)^2} {}^nR_i^m\right] \tag{4- 40}$$

and $${}^{n}R_i^m = \frac{{}^{n}x_i^m - {}^{n}y_i^m}{r_n^m}$$

4.5 Displacement and Stress Green's Functions in Solids

As discussed in Chapter 3, the equation of motion written in terms of the displacement is called Navier's equation. In vector notion, Navier's equation can be written as

$$(\lambda + 2\mu)\underline{\nabla}(\underline{\nabla}.\mathbf{u}) - \mu\underline{\nabla} \times (\underline{\nabla} \times \mathbf{u}) + \mathbf{f} = \rho\ddot{\mathbf{u}} \tag{4- 41}$$

Dividing equation 4-42 by ρ, it becomes

$$\frac{(\lambda + 2\mu)}{\rho}\underline{\nabla}(\underline{\nabla}.\mathbf{u}) - \frac{\mu}{\rho}\underline{\nabla} \times (\underline{\nabla} \times \mathbf{u}) + \frac{\mathbf{f}}{\rho} = \ddot{\mathbf{u}} \tag{4- 42}$$

Recall the longitudinal (P-wave) speed and transverse (S-wave) speed in homogeneous isotropic materials are $c_p = \sqrt{\frac{\lambda+2\mu}{\rho}}$ and $c_s = \sqrt{\frac{\lambda}{\rho}}$ respectively. Then,

$$c_p^2\underline{\nabla}(\underline{\nabla}.\mathbf{u}) - c_s^2\underline{\nabla} \times (\underline{\nabla} \times \mathbf{u}) + \frac{\mathbf{f}}{\rho} = \ddot{\mathrm{u}} \tag{4- 43}$$

It is also shown in Chapter 3 that Helmholtz decomposition allows one to express the displacement vector field in terms of two potentials: a scalar potential and a vector potential. Since any scalar potential can be written as the divergence of a vector potential, and any vector potential may be expressed as the curl of another vector potential, the displacement vector field can be written in terms of two vector potentials. Thus,

$$\mathbf{u} = \underline{\nabla}\left(\underline{\nabla}.\Phi\right) - \underline{\nabla} \times \left(\underline{\nabla} \times \Psi\right) \tag{4- 44}$$

Where ϕ and ψ are vector potentials and are functions of time and space. Note that, $\varphi = \underline{\nabla}.\phi$ and $A = -\nabla \times \psi$ in equation 3-10. Substituting equation 4-45 into equation 4-44 gives

$$\underline{\nabla\nabla}.\left(c_p^2\nabla^2\mathbf{\Phi} - \ddot{\mathbf{\Phi}}\right) - \underline{\nabla} \times \underline{\nabla} \times \left(c_s^2\nabla^2\mathbf{\Psi} - \ddot{\mathbf{\Psi}}\right) + \frac{\mathbf{f}}{\rho} = 0 \tag{4- 45}$$

Note that, ϕ is irrotational $\left(\underline{\nabla} \times \phi = 0\right)$, and ψ is solenoidal $\left(\underline{\nabla}.\psi = 0\right)$ by definition of Helmholtz decomposition. In deriving equation 4-46, the following vector identity is also used:

$$\nabla^2\mathrm{v} = \underline{\nabla}\left(\underline{\nabla}.\mathbf{v}\right) - \underline{\nabla} \times \underline{\nabla} \times \mathbf{v} \tag{4- 46}$$

4.5.1 Point Source in Solids

The fundamental solution (Green's Function) of Equation 4-46 is the response in a solid medium due to the excitation caused by a point source. The point source excitation contributes to the body force term in Equation 4-46 as a concentrated impulse force. Without the loss of generality, the body force term can be expressed as

$$\mathbf{f}(x,t) = \mathbf{P}f(t)\delta(\mathbf{x})$$

or

$$f_i = P_i f(t)\delta\left(\mathbf{x}_j\right) \tag{4- 47}$$

where, P is the force vector with no temporal or spatial dependence and δ(x) is the Dirac-delta function.

In order to further simplify Equation 4-46, one can focus on the spatial derivative of the potentials. Poisson's equation, $\nabla^2 \emptyset = q(x)$ has the general solution of

$$\emptyset = -\frac{1}{4\pi}\int_V \frac{q(y)}{|\mathbf{x}-\mathbf{y}|}dV \tag{4- 48}$$

For $q(x) = \delta(x)$, the following property of Dirac-delta function

$$\int_V g(\mathbf{x})\delta(\mathbf{x})dV = g(0)$$

Can be utilized to simplify equation 4-49 to

$$\phi = -\frac{1}{4\pi}\frac{1}{|\mathbf{x}|} = -\frac{1}{4\pi|\mathbf{x}|} \tag{4- 49}$$

Substituting equation 3-50 into the Poisson's equation gives:

$$\nabla^2 \emptyset = \nabla^2\left(-\frac{1}{4\pi r}\right) = q(\mathbf{x}) = \delta(\mathbf{x}) \tag{4- 50}$$

Where $r = |x|$ for a source at the origin.

Using the above expression of δ(x) and the vector identity (equation 4-47), one can write equation 4-48 as

$$\mathbf{f} = -\mathbf{P}\nabla^2\left(\frac{f(t)}{4\pi r}\right) = \mathbf{P}\left\{\nabla\left[\underline{\nabla}.\left(\frac{f(t)}{4\pi r}\right)\right] - \underline{\nabla}\times\left[\underline{\nabla}\times\left(\frac{f(t)}{4\pi r}\right)\right]\right\} \tag{4- 51}$$

The two vector potentials, ϕ and ψ, without any loss of generality, can be written in terms of two scalar potentials of the form

$$\mathbf{\Phi} = \mathbf{P}\phi$$

$$\mathbf{\Psi} = \mathbf{P}\psi \tag{4- 52}$$

Substituting equations 4-52 and 4-53 into equation 4-46,

$$\underline{\nabla\nabla}.\mathbf{P}\left(c_p^2\nabla^2\phi - \ddot{\phi} - \frac{f(t)}{4\pi r\rho}\right) - \underline{\nabla}\times\underline{\nabla}\times\mathbf{P}\left(c_s^2\nabla^2\psi - \ddot{\psi} - \frac{f(t)}{4\pi r\rho}\right) = 0 \tag{4- 53}$$

For harmonic time dependency $\left(e^{-i\omega t}\right)$ of the point source, other variables can also be assumed to be harmonic and they can be expressed as

$$\phi(x_j,t) = \phi(x_j)e^{-i\omega t}$$

$$\psi(x_j,t) = \psi(x_j)e^{-i\omega t}$$

$$u_i(x_j,t) = U_i(x_j)e^{-i\omega t}$$

Replacing these expressions in equation 4-54

$$\underline{\nabla}\,\underline{\nabla}.\mathbf{P}\left(c_p^2\nabla^2\phi + \omega^2\phi - \frac{1}{4\pi r\rho}\right)e^{-i\omega t} - \underline{\nabla}\times\underline{\nabla}\times\mathbf{P}\left(c_s^2\nabla^2\psi - \omega^2\psi - \frac{1}{4\pi r\rho}\right)e^{-i\omega t} = 0 \tag{4- 54}$$

This equation can be satisfied with the following sufficient conditions:

$$\nabla^2\phi + \frac{\omega^2}{c_p^2}\phi = \frac{1}{4\pi r c_p^2\rho} \tag{4- 55}$$

$$\nabla^2\psi - \frac{\omega^2}{c_p^2}\psi = \frac{1}{4\pi r c_s^2 \rho} \tag{4- 56}$$

From Mal and Singh [90], particular solutions of equations 4-56 and 4-57 can be written as

$$\phi = \frac{1 - e^{-ik_p r}}{4\pi\rho\omega^2 r} \tag{4- 57}$$

And

$$\psi = \frac{1 - e^{-ik_s r}}{4\pi\rho\omega^2 r} \tag{4- 58}$$

Where, $k_p = \frac{\omega}{c_p}$ and $k_s = \frac{\omega}{c_s}$.

4.5.2 Displacement Field in Solids

By substituting Equations 4-58 and 4-59 into Equation 4-45, the displacement field can be expressed in terms of force vector **P** and the properties of the solid medium as

$$\mathbf{u} = \mathbf{U}e^{-i\omega t} = \underline{\nabla}\left[\underline{\nabla}.\mathbf{P}\left(\frac{1 - e^{ik_p r}}{4\pi\rho\omega^2 r}\right)\right]e^{-i\omega t} - \underline{\nabla}\times\left[\underline{\nabla}\times\mathbf{P}\left(\frac{1 - e^{ik_s r}}{4\pi\rho\omega^2 r}\right)\right]e^{-i\omega t} \tag{4- 59}$$

Using the vector identity equation 4-47 modifies equation 4-60 to

$$\mathbf{u} = \mathbf{U}e^{-i\omega t} = \underline{\nabla}\left[\underline{\nabla}.\mathbf{P}\left(\frac{1-e^{ik_p r}}{4\pi\rho\omega^2 r}\right)\right]e^{-i\omega t} + \nabla^2\mathbf{P}\left(\frac{1-e^{ik_s r}}{4\pi\rho\omega^2 r}\right) - \underline{\nabla}\left[\underline{\nabla}.\mathbf{P}\left(\frac{1-e^{ik_s r}}{4\pi\rho\omega^2 r}\right)\right]e^{-i\omega t} \tag{4- 60}$$

Or

$$\mathbf{u} = \mathbf{U}e^{-i\omega t} = \underline{\nabla}\left[\underline{\nabla}.\mathbf{P}\left(\frac{e^{ik_p r} - e^{ik_s r}}{4\pi\rho\omega^2 r}\right)\right]e^{-i\omega t} + \nabla^2\mathbf{P}\left(\frac{1 - e^{ik_s r}}{4\pi\rho\omega^2 r}\right) \tag{4- 61}$$

Applying the Laplace operator on the second term in equation 4-62,

$$\mathbf{u} = \mathbf{U}e^{-i\omega t} = \underline{\nabla}\left[\underline{\nabla}.\mathbf{P}\left(\frac{e^{ik_p r} - e^{ik_s r}}{4\pi\rho\omega^2 r}\right)\right]e^{-i\omega t} + \left(\frac{\mathbf{P}e^{ik_s r}}{4\pi\rho\omega^2 r}k_s^2\right)e^{-i\omega t} = [\mathbf{G}(\mathbf{x};0)\mathbf{P}]e^{-i\omega t} \tag{4- 62}$$

In index notation, the spatial part U of the displacement expression in $\mathbf{u} = Ue^{-i\omega t}$ can be written as

$$\begin{aligned} U_i &= \frac{1}{4\pi\rho\omega^2}\left[k_s^2\frac{e^{ik_s r}}{r}P_i - \frac{\partial^2}{\partial x_i \partial x_j}\left(P_j\frac{e^{ik_p r} - e^{ik_s r}}{r}\right)\right] \\ &= \frac{1}{4\pi\rho\omega^2}\left[k_s^2\frac{e^{ik_s r}}{r}\delta_{ij} - \frac{\partial^2}{\partial x_i \partial x_j}\left(\frac{e^{ik_p r} - e^{ik_s r}}{r}\right)P_j\right] = G_{ij}(\mathbf{x};0)P_j \end{aligned} \tag{4- 63}$$

Equations 4-63 and 4-64 are the expressions of the displacement at point x due to a point source located at the origin. The response at point **x** due to a point source placed at coordinate **y** is

$$u_i = U_i e^{-i\omega t} = G_{ij}(\mathbf{x};\mathbf{y})P_j e^{-i\omega t} \tag{4- 64}$$

G_{ij} (x;y) is regarded as the space dependent Green's function of displacement for homogeneous isotropic solids. Substituting $r = |x - y|$ for the distance between a target point and source point, the Green's function can be written as [90],

$$G_{ij}(\mathbf{x};\mathbf{y}) = \frac{1}{4\pi\rho\omega^2}\begin{Bmatrix} \frac{e^{ik_p r}}{r}\left[k_p^2 R_i R_j + \left(3R_i R_j - \delta_{ij}\right)\left(\frac{ik_p}{r} - \frac{1}{r^2}\right)\right] + \\ \frac{e^{ik_s r}}{r}\left[k_s^2\left(\delta_{ij} - R_i R_j\right) - \left(3R_i R_j - \delta_{ij}\right)\left(\frac{ik_s}{r} - \frac{1}{r^2}\right)\right] \end{Bmatrix} \quad (4\text{- }65)$$

Where $R_i = \frac{x_i - y_i}{r}$

In matrix form

$$\mathbf{G}(\mathbf{x};\mathbf{y}) = [\mathbf{G_1}(\mathbf{x};\mathbf{y}) \quad \mathbf{G_2}(\mathbf{x};\mathbf{y}) \quad \mathbf{G_3}(\mathbf{x};\mathbf{y})]^{\mathbf{T}}$$

And

$$\mathbf{u} = [\mathbf{G}(\mathbf{x};\mathbf{y})\mathbf{P}]e^{-i\omega t} \quad (4\text{- }66)$$

Note that a point source with unit excitation force at y acting in the *j*-th direction produces the displacement $G_{ij}(x;y)$ in the *i*-th direction at point x.

4.5.3 Stress Field in Solids

Recall the strain-displacement relation (equation 1-3). Using equation 4-65, it can be expressed in terms of displacement Green's function as

$$\varepsilon_{ij} = \frac{1}{2}\left(G_{ij,k} + G_{jk,i}\right)P_k \quad (4\text{- }67)$$

Note that the harmonic time dependency is implied in Equation 4-68. Henceforth, the time dependency is always implied unless it is otherwise specified. The relation between stress and strain called the constitutive law for linear elastic material is

$$\sigma_{ij} = C_{ijkl}\varepsilon_{kl} \quad (4\text{- }68)$$

The stress at position **x** due to a concentrated force at **y** can be expressed in terms of Green's function by substituting Equation 4-68 into Equation 4-69,

$$S_{ij}(\mathbf{x};\mathbf{y}) = \frac{1}{2}C_{ijkl}\left(G_{kq,l} + G_{lq,k}\right)P_q \tag{4- 69}$$

On the other hand, recall $\sigma_{ij} = 2\mu\varepsilon_{ij} + \lambda\varepsilon_{kk}\delta_{ij}$ (Equation 1-2). Therefore, the stress at point **x** due to a force at point **y** can also be expressed as

$$S_{ij}(\mathbf{x};\mathbf{y}) = \mu\left(G_{ik,j} + G_{jk,i}\right)P_k + \lambda G_{kq,k}P_q\delta_{ij} \tag{4- 70}$$

Or

$$S_{ij}(\mathbf{x};\mathbf{y}) = \left[\mu\left(G_{ik,j} + G_{jk,i}\right)\delta_{kq} + \lambda G_{kq,k}P_q\delta_{ij}\right]P_q \tag{4- 71}$$

When all differentiations of the Green's function in the above equation are carried out, the components of stress (σ_{ij}) at point **x** generated by a concentrated force of unit amplitude acting at point y in the x_m –direction is denoted by σ_{ij}^m whose components can be expressed as

$$\sigma_{11}^1 = (2\mu + \lambda)(G_{11}d_1) + \lambda(G_{21}d_2 + G_{31}d_3) \tag{4- 72}$$

$$\sigma_{11}^2 = (2\mu + \lambda)(G_{12}d_1) + \lambda(G_{22}d_2 + G_{32}d_3) \tag{4- 73}$$

$$\sigma_{11}^3 = (2\mu + \lambda)(G_{13}d_1) + \lambda(G_{23}d_2 + G_{33}d_3) \tag{4- 74}$$

$$\sigma_{33}^1 = (2\mu + \lambda)(G_{31}d_3) + \lambda(G_{11}d_1 + G_{21}d_2) \tag{4- 75}$$

$$\sigma_{33}^2 = (2\mu + \lambda)(G_{32}d_3) + \lambda(G_{12}d_1 + G_{22}d_2) \tag{4- 76}$$

$$\sigma_{33}^{3} = (2\mu + \lambda)(G_{33}d_3) + \lambda(G_{13}d_1 + G_{23}d_2) \quad (4\text{- }77)$$

$$\sigma_{31}^{1} = \mu(G_{31}d_1 + G_{11}d_3) \quad (4\text{- }78)$$

$$\sigma_{31}^{2} = \mu(G_{32}d_1 + G_{12}d_3) \quad (4\text{- }79)$$

$$\sigma_{31}^{3} = \mu(G_{33}d_1 + G_{13}d_3) \quad (4\text{- }80)$$

$$\sigma_{32}^{1} = \mu(G_{31}d_2 + G_{21}d_3) \quad (4\text{- }81)$$

$$\sigma_{32}^{2} = \mu(G_{32}d_2 + G_{22}d_3) \quad (4\text{- }82)$$

$$\sigma_{32}^{3} = \mu(G_{33}d_2 + G_{23}d_3) \quad (4\text{- }83)$$

The detailed derivation of equation 4-73 through 4-84 is given in Appendix A.

4.6 Displacement and Stress Fields in Solids Due to Multiple Point Sources

When a number of point sources generate an excitation in a solid medium, the response at any point in the medium can be determined by superposition of the contributions from every point source. If *N* number of point sources are used to express the excitation in a solid as shown in Figure 4.4, the displacement at point **x** can be expressed simply by summing all individual contributions. Therefore, based on Equation 4-65 or 4-67, the expressions for displacement components at point **x** due to N number of point sources are given by

$$u_1 = \sum_{m=1}^{N} (G_{11}^m P_1^m + G_{12}^m P_2^m + G_{13}^m P_3^m) = \sum_{m=1}^{N} \mathbf{G}_1^m \mathbf{P}^{\mathrm{m}} \tag{4- 84}$$

$$u_2 = \sum_{m=1}^{N} (G_{21}^m P_1^m + G_{22}^m P_2^m + G_{23}^m P_3^m) = \sum_{m=1}^{N} \mathbf{G}_2^{\mathrm{m}} \mathbf{P}^{\mathrm{m}} \tag{4- 85}$$

$$u_3 = \sum_{m=1}^{N} (G_{31}^m P_1^m + G_{32}^m P_2^m + G_{33}^m P_3^m) = \sum_{m=1}^{N} \mathbf{G}_3^m \mathbf{P}^{\mathrm{m}} \tag{4- 86}$$

where G_{ij}^m is equal to G_{ij} given in equation 4-66 for the m-th point source.

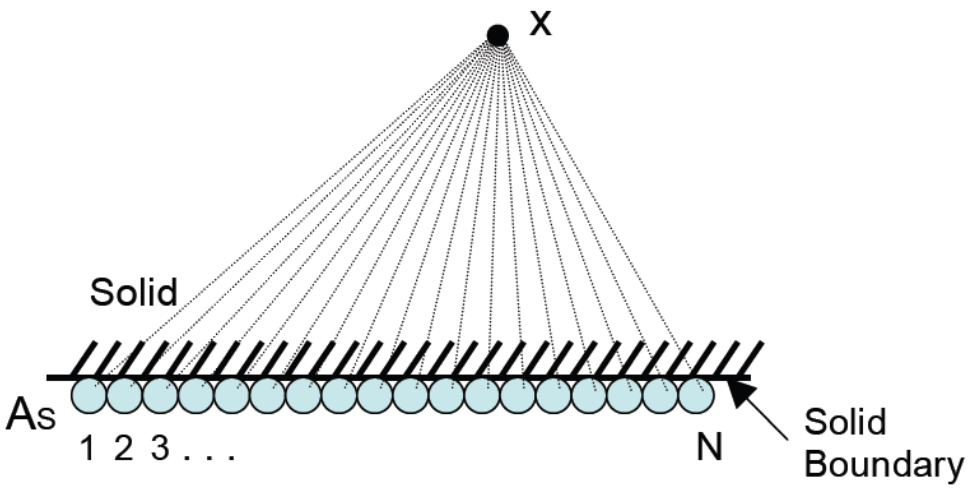

Figure 4.4 Group of point sources at the solid boundary contributing to the field at point *T*

Similarly, using Equations 4-73 through 4-84, one can compute stress components at point **x** when a group of concentrated forces are contributing. Superimposing all the contributions from all *N* point sources results in the total stress at point **x** as

$$S_{ij} = \sum_{m=1}^{N} S_{ij}^{m}(\mathbf{x}; \mathbf{y_m})$$

$$= \sum_{m=1}^{N} \left[\left(\sigma_{ij}^{1}\right)^{m} P_1^m + \left(\sigma_{ij}^{2}\right)^{m} P_2^m + \left(\sigma_{ij}^{3}\right)^{m} P_3^m \right] = \sum_{m=1}^{N} \mathbf{s}_{ij}^{m} \mathbf{P}_{\mathrm{m}} \tag{4- 87}$$

Where

$$\mathbf{s}_{ij}^{m} = \left[\left(\sigma_{ij}^{1}\right)^{m} \quad \left(\sigma_{ij}^{2}\right)^{m} \quad \left(\sigma_{ij}^{3}\right)^{m} \right] \tag{4- 88}$$

$$\mathbf{P}^{\mathrm{m}} = [P_1^m \quad P_2^m \quad P_3^m] \tag{4- 89}$$

Note that m-th concentric force (point source) has the force components P_1^m, P_2^m and P_3^m in the x_1, x_2 and x_3 directions, respectively.

4.6.1 Matrix Representation

In order to obtain the total ultrasonic fields in a solid medium, it is necessary to determine the fields at multiple target points. Assuming that *N* source points emulate the excitation in a solid and that there are *M* target points in the solid where the field is to be computed, the i-th component of displacement at M target points forms a $M \times 1$ vector.

$$\mathbf{u}_i = [u_1^1 \quad u_1^2 \quad u_1^3 \quad \ldots \quad u_1^{N-1} \quad u_1^N]^T \tag{4- 90}$$

where i = 1, 2, 3. The element u_i^n is the displacement at *n*-th target point in the *i*-th direction. Due to Equation 4-85, 4-86, and 4-87, one can determine u_i vector by

$$\mathbf{u}_{\mathrm{i}} = [\mathbf{DS_i}]\mathbf{A} \tag{4- 91}$$

where,

$$[\mathbf{DS_i}] = \begin{bmatrix} {}^{1}\mathbf{G}_{\mathrm{i}}^{1} & {}^{1}\mathbf{G}_{\mathrm{i}}^{2} & {}^{1}\mathbf{G}_{\mathrm{i}}^{3} & \dots & {}^{1}\mathbf{G}_{\mathrm{i}}^{\mathrm{N}-1} & {}^{1}\mathbf{G}_{\mathrm{i}}^{\mathrm{N}} \\ {}^{2}\mathbf{G}_{\mathrm{i}}^{1} & {}^{2}\mathbf{G}_{\mathrm{i}}^{2} & {}^{2}\mathbf{G}_{\mathrm{i}}^{3} & \dots & {}^{2}\mathbf{G}_{\mathrm{i}}^{\mathrm{N}-1} & {}^{2}\mathbf{G}_{\mathrm{i}}^{\mathrm{N}} \\ {}^{3}\mathbf{G}_{\mathrm{i}}^{1} & {}^{3}\mathbf{G}_{\mathrm{i}}^{2} & \dots & \dots & \dots & {}^{3}\mathbf{G}_{\mathrm{i}}^{\mathrm{N}} \\ \dots & \dots & \dots & \dots & \dots & \dots \\ {}^{\mathrm{M}-1}\mathbf{G}_{\mathrm{i}}^{1} & {}^{\mathrm{M}-1}\mathbf{G}_{\mathrm{i}}^{2} & \dots & \dots & {}^{\mathrm{M}-1}\mathbf{G}_{\mathrm{i}}^{\mathrm{N}-1} & {}^{\mathrm{M}-1}\mathbf{G}_{\mathrm{i}}^{\mathrm{N}} \\ {}^{\mathrm{M}}\mathbf{G}_{\mathrm{i}}^{1} & {}^{\mathrm{M}}\mathbf{G}_{\mathrm{i}}^{2} & \dots & \dots & {}^{\mathrm{M}}\mathbf{G}_{\mathrm{i}}^{\mathrm{N}-1} & {}^{\mathrm{M}}\mathbf{G}_{\mathrm{i}}^{\mathrm{N}} \end{bmatrix}_{(\mathrm{M}\times 3\mathrm{N})} \tag{4- 92}$$

And

$$\mathbf{A} = [(\mathbf{P}^{1})^{\mathrm{T}} \quad (\mathbf{P}^{2})^{\mathrm{T}} \quad (\mathbf{P}^{3})^{\mathrm{T}} \quad \dots \quad \dots \quad \dots \quad (\mathbf{P}^{\mathrm{N}-1})^{\mathrm{T}} \quad (\mathbf{P}^{\mathrm{N}})^{\mathrm{T}}] \tag{4- 93}$$

${}^{p}G_{i}^{q}$ is displacement Green's function at p-th target point due to q-th point source. $\left(\mathbf{P}^{i}\right)^{T}$ is the transpose of 3×1 vector defined in Equation 4-90 for the i-th point source.

In addition, each stress component at M target points forms a $M \times 1$ vector given by the following expression:

$$\mathbf{s}_{\mathrm{ij}} = \left[\mathbf{s}_{\mathrm{ij}}^{1} \quad \mathbf{s}_{\mathrm{ij}}^{2} \quad \mathbf{s}_{\mathrm{ij}}^{3} \quad \dots \quad \dots \quad \mathbf{s}_{\mathrm{ij}}^{\mathrm{M}-1} \quad \mathbf{s}_{\mathrm{ij}}^{\mathrm{M}}\right]^{\mathrm{T}} \tag{4- 94}$$

where s_{ij}^{m} is defined in equation 4-89. s_{ij} vector can be computed from

$$\mathbf{s}_{\mathrm{ij}} = \left[\mathbf{S}_{\mathrm{ij}}\right]\mathbf{A} \tag{4- 95}$$

where A is defined in equation 4-94 and S_{ij} is given by

$$[\mathbf{S}_{ij}] = \begin{bmatrix} {}^{1}\mathbf{s}_{ij}^{1} & {}^{1}\mathbf{s}_{ij}^{2} & {}^{1}\mathbf{s}_{ij}^{3} & \dots & {}^{1}\mathbf{s}_{ij}^{N-1} & {}^{1}\mathbf{s}_{ij}^{N} \\ {}^{2}\mathbf{s}_{ij}^{1} & {}^{2}\mathbf{s}_{ij}^{2} & {}^{2}\mathbf{s}_{ij}^{3} & \dots & {}^{2}\mathbf{s}_{ij}^{N-1} & {}^{2}\mathbf{s}_{ij}^{N} \\ {}^{3}\mathbf{s}_{ij}^{1} & {}^{3}\mathbf{s}_{ij}^{2} & \dots & \dots & \dots & {}^{3}\mathbf{s}_{ij}^{N} \\ \dots & \dots & \dots & \dots & \dots & \dots \\ {}^{M-1}\mathbf{s}_{ij}^{1} & {}^{M-1}\mathbf{s}_{ij}^{2} & \dots & \dots & {}^{M-1}\mathbf{s}_{ij}^{N-1} & {}^{M-1}\mathbf{s}_{ij}^{N} \\ {}^{M}\mathbf{s}_{ij}^{1} & {}^{M}\mathbf{s}_{ij}^{2} & \dots & \dots & {}^{M}\mathbf{s}_{ij}^{N-1} & {}^{M}\mathbf{s}_{ij}^{N} \end{bmatrix}_{(M\times 3N)} \quad (4\text{- }96)$$

Note that ${}^{p}s_{ij}^{q}$ is the stress component ij (σ_{ij}) at p-th target point due to q-th point source.[46]

CHAPTER 5

MODELLING OF TRANSDUCER OF AN ACOUSTIC MICROSCOPE

Acoustic microscopy is a popular technique for characterization of biological tissues and cells. There are three basic types of acoustic microscope: (i) Scanning Acoustic Microscope (SAM), (ii) Scanning Laser Acoustic Microscope (SLAM) and (iii) C-mode Scanning Acoustic Microscope (C-SAM).

SLAM uses the principles of plane wave sound propagation for imaging and quantification of acoustic properties [91]. A scanning laser detection system is used here for capturing the wave signals optically. While SAM's output is the amplitude of either reflected or transmitted wave by a specimen at a particular point [92], the C-SAM uses C-scan mode which provides a planar view image at a particular depth [93]. The microscope can operate either on reflection-mode, or in transmission mode. In reflection mode, the microscope can capture the reflected wave as the output signal, whereas, in transmission mode, the transmitted wave is detected by a secondary transducer placed behind a sample. Acoustic microscopy is especially powerful at high frequencies, *i.e*, around 1 GHz, which can be used for high resolution imaging, material characterization or biological cell property determination.

Focused ultrasonic waves with high spatial resolution can be used to determine the mechanical properties of samples such as living cells [94-99]. Samples are submerged in a liquid medium such as distilled water or alcohol to ensure the acoustic waves are delivered to and from the samples (acoustic waves propagates most efficiently through liquid and solid materials). Therefore, modelling of ultrasonic fields generated by a transducer of finite dimension which is immersed in fluid medium is an important fundamental problem. Due to its timeless appeal as well as numerous practical applications, it continues to inspire many researchers to work on finding a better solution. There are numerous publications for generalized expressions derived by rigorous mathematical theories [66, 73, 74]. As an alternative and more efficient method, DPSM is used to compute the ultrasonic field. But due to its requirement of rigorous understanding, most of the previous works was done with single surface of the transducer, whereas, the actual transducer used for acoustic microscopy is not consisted of only one surface. This real life modelling shows an agreement with design specification of the transducer.

5.1 Problem Description

The objective of this problem is to model the ultrasonic field generated by ultrasonic transducers of finite dimension when the transducer are immersed partially on a fluid. Thus, it numerically simulates the pupil function and focusing of the ultrasonic beam emanating from a SAM transducers, which can be further used for the cell property determination.

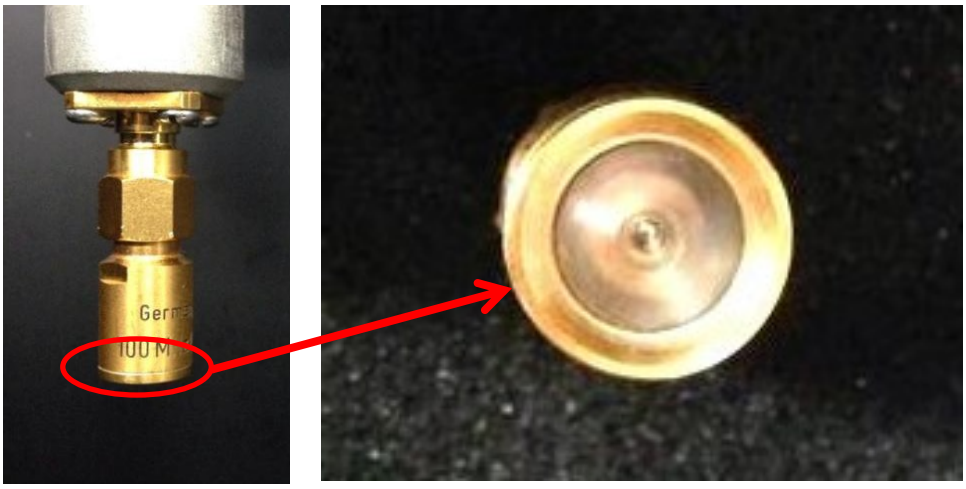

(a) (b)

Figure 5.1 (a) Side view of the Acoustic Microscope Lens,

(b) 100 MHz lens tip

The side view of the acoustic microscope lens is shown in the photograph presented in fig 5-1(a) and image of the lens tip in shown in fig 5-1(b). The dark circular region at the center of the acoustic image of figure 5-1(b) corresponds to the concave lens.

The illustration of this particular acoustic microscope lens is shown in figure 5-2. It has four different type of geometrical configuration. The top surface of the lens rod is a circular portion on which a transducer is mounted. The lens rod is a cylindrical portion, and after the cylinder part, there is a conical part. At the end of the conical part, the concave lens is situated.

The geometry and the dimension of the lens as manufactured are presented in table 5.1.

Table 5.1: Geometry and dimension of the lens

Geometrical Shape	Position	Dimension
Circular part	Position A Surface 1	Diameter = 6.5 mm
Cylindrical part	Position B Surface 2	Diameter = 6.5 mm Height= 4 mm
Conical part	Position C Surface 3	Top end Dia = 6.5 mm Height= 0.407 Opening angle=100°
Concave lens	Position D Surface 4	Sphere dia= 1.140 mm Opening angle=100°

Figure 5-2 shows the position of liquid relative to the lens rod. The focused lens has a radius of curvature r. Its center of curvature is located at point E and the focal point is F.

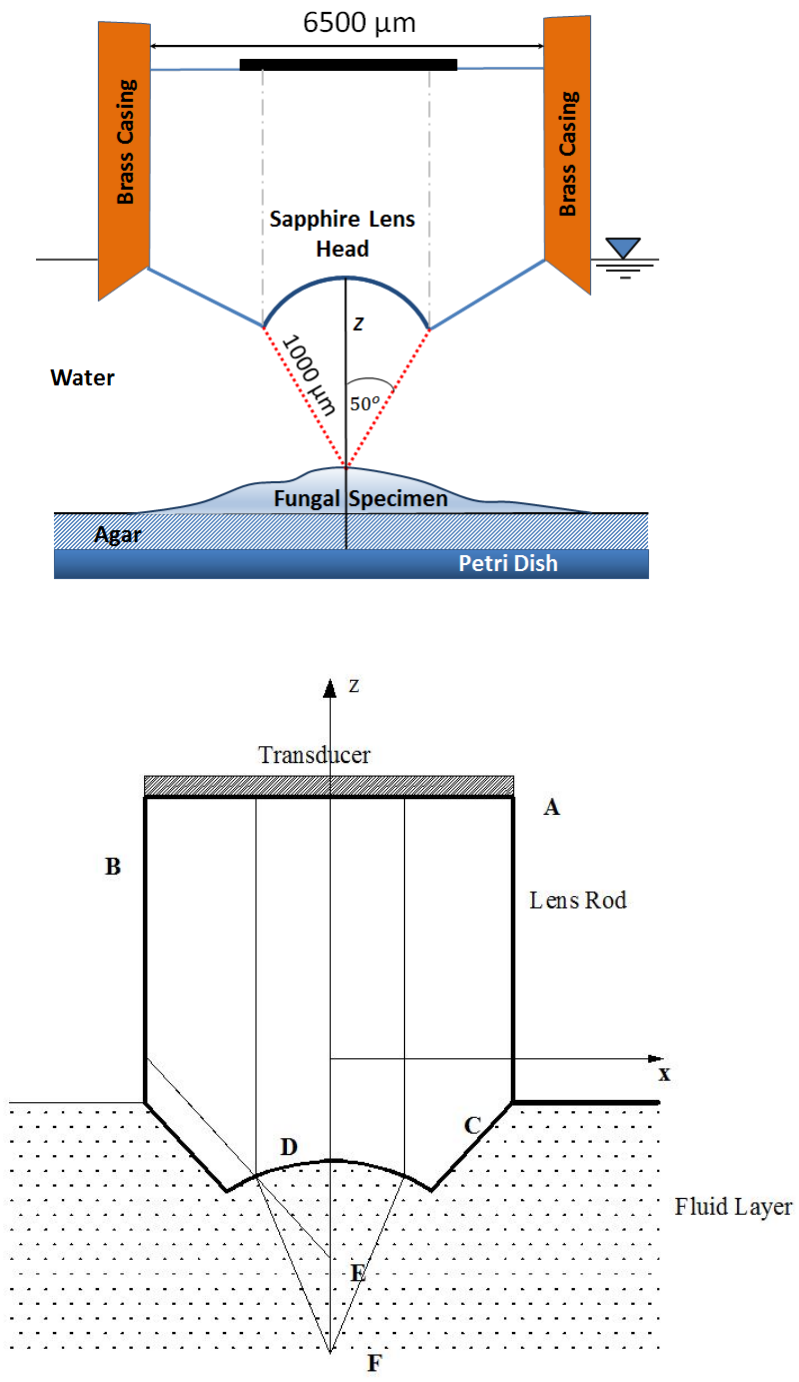

Figure 5.2 Schematic of the acoustic microscope inspecting a solid surface submerged in fluid layer. A is a point located in surface 1, B in surface 2, C in surface 3 and D in surface 4. E is the center of curvature of the lens, F is the focal point.

A number of point sources are distributed over the surfaces. Depending on the influence of the point sources, source distribution is done on either one side or both side of the surface. These sources, when superimposed, should produce the total ultrasonic field in the fluid and the solid media. The distribution of point sources is shown in figure 5-3. On the flat end of the lens rod, the ultrasonic transducer (signal generator) is mounted. The end is denoted as surface 1. A layer of point source denoted by A_1 is distributed on this surface. The ultrasonic signal that is generated by the transducer is propagated through the lens rod. Thus the surface of the lens rod has an impact on the propagation. Hence, a layer of point source outside the surface has been distributed, and the sources are denoted by A_2. The third surface is the conical portion, and from this portion, the lens is submerged in fluid. Part of the signal energy is reflected back into the solid lens material (Medium 1) and part is transmitting through the fluid and the solid layer ahead. So, the distribution of point sources is necessary on both sides of the surface. Hence, two layers of point source, named A_3 and A_3^*, are positioned here.

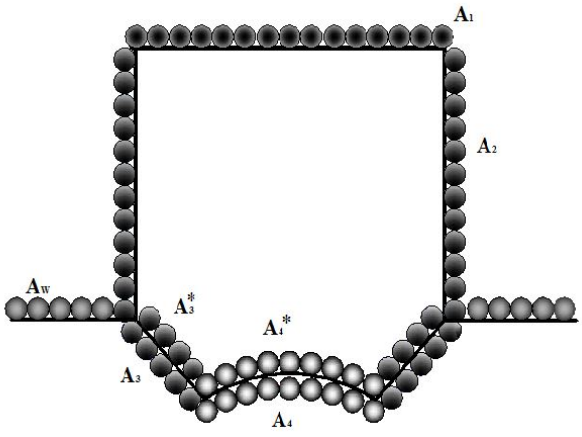

Figure 5.3 Point source distribution relative to the lens geometry for the DPSM modeling of the acoustic lens

One layer (A_3^*) models the transmitted field in fluid layer and the other layer (A_3) models the reflected field inside the lens rod. Then the ultrasonic signal strikes the concave surface of the lens. Similar to surface 3, two layers of point sources has been distributed along surface 4, as A_4 and A_4^*. Note that, for this problem, uniformly distributed point sources have been used as shown in figure 5-3. Figure 5-4 shows the point source distribution in different surface of the lens body.

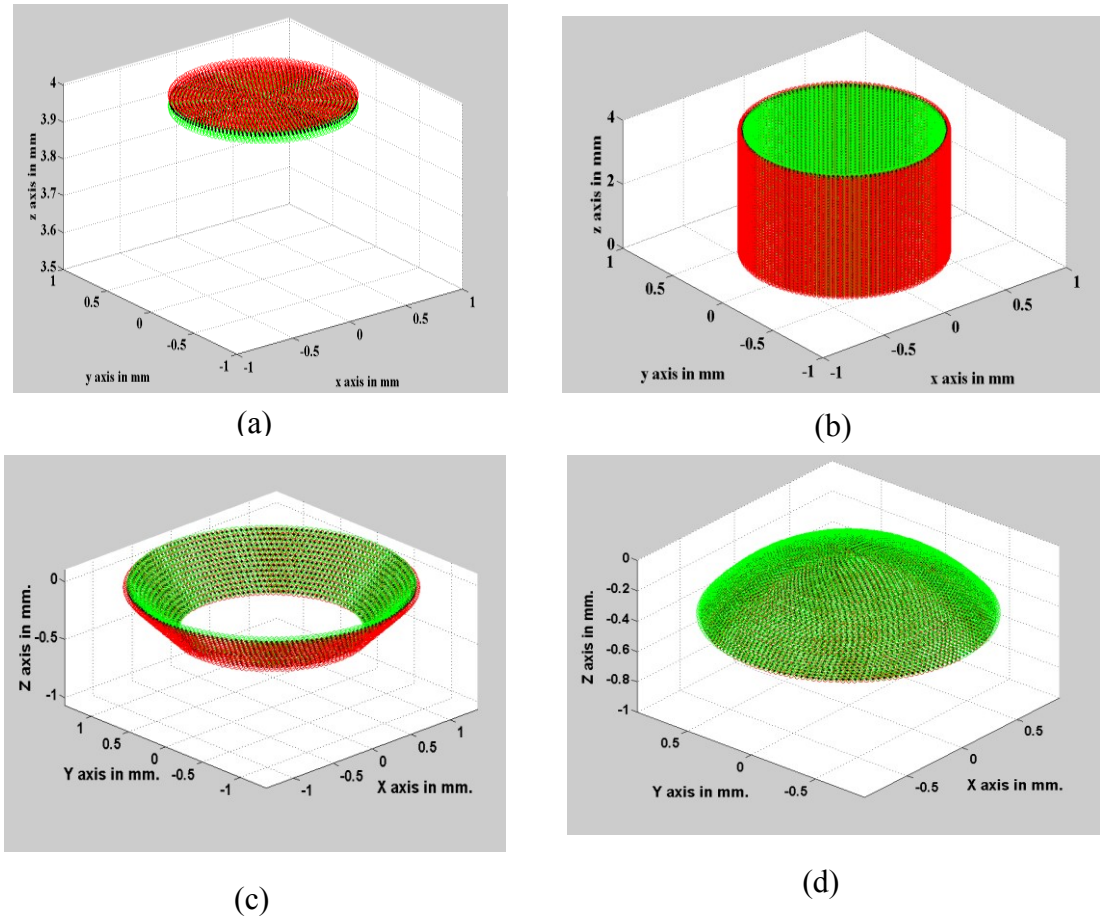

Figure 5.4 Distribution of point sources over the acoustic lens surface;
(a) Surface 1 – Circular surface; (b) Surface 2 – Cylindrical surface;
(c) Surface 3 – Conical surface; (d) Surface 4 – Concave lens.
(Not to Scale)

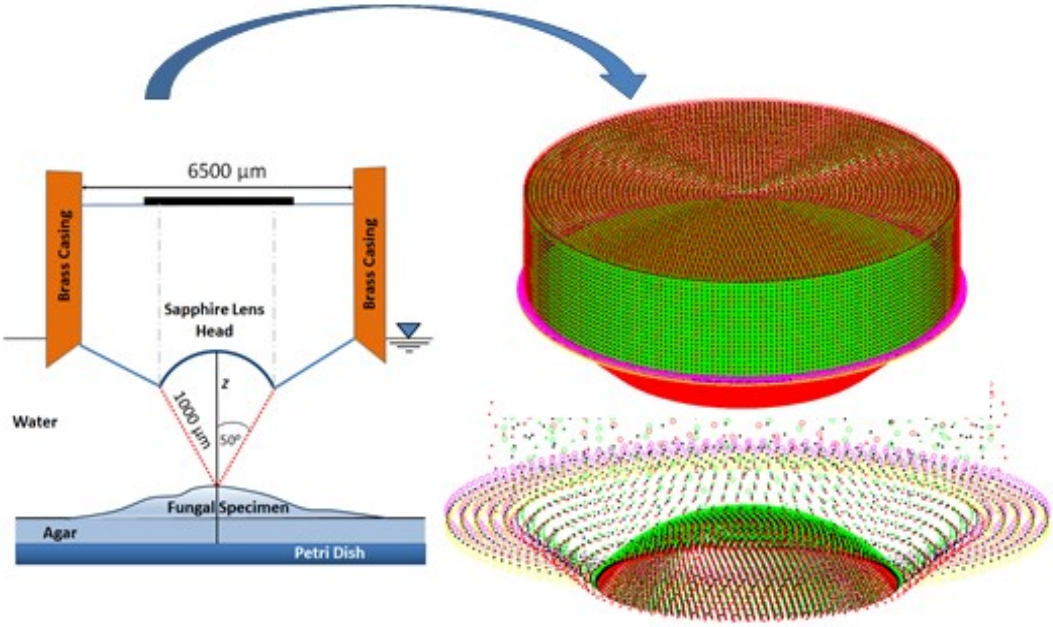

Figure 5.5 Distribution of point sources over the whole surface

5.2 Matrix Formulation to Calculate Source Strengths

Every point source considered to calculate the transmitted field in the solid has three different point forces in three mutually perpendicular directions as unknowns. If the number of target points is *M* for any surface, the displacement due to *N* number of point sources at the surface are related to the point source strength and is an $M \times 3N$ matrix. From equation (4-92), the displacement in three directions at surface 1 (the set of target point called *I*1) due to A_1, A_2, A_3 & A_4 source strength vector can be written as:

$$u3_{I1} = DS3_{11}A_1 + DS3_{12}A_2 + DS3_{13}A_3 + DS3_{14}A_4 \quad (5\text{- }1)$$

$$u1_{I1} = DS1_{11}A_1 + DS1_{12}A_2 + DS1_{13}A_3 + DS1_{14}A_4 \quad (5\text{- }2)$$

$$u2_{I1} = DS2_{11}A_1 + DS2_{12}A_2 + DS2_{13}A_3 + DS2_{14}A_4 \quad (5\text{- }3)$$

For surface 2, the surface is a nonplaner surface, and for that, at every point of the interface, normal stress relative to the surface need to be defined to satisfy the continuity condition across the surface. When the point source is acting at y in an isotropic solid, the stress develops at point x can be written as follows:

$$\sigma_j = \begin{bmatrix} \sigma_{11}^j & \sigma_{12}^j & \sigma_{13}^j \\ \sigma_{21}^j & \sigma_{22}^j & \sigma_{23}^j \\ \sigma_{31}^j & \sigma_{32}^j & \sigma_{33}^j \end{bmatrix}$$

For this surface, angle between x- and y- direction in θ, the transformation matrix at any point x should be:

$$T = \begin{bmatrix} cos\theta & sin\theta & 0 \\ -sin\theta & cos\theta & 0 \\ 0 & 0 & 1 \end{bmatrix}$$

Therefore, transformed stresses for point x is:

$$\sigma'^j = T\sigma_j T^T = \begin{bmatrix} cos\theta & sin\theta & 0 \\ -sin\theta & cos\theta & 0 \\ 0 & 0 & 1 \end{bmatrix} \begin{bmatrix} \sigma_{11}^j & \sigma_{12}^j & \sigma_{13}^j \\ \sigma_{21}^j & \sigma_{22}^j & \sigma_{23}^j \\ \sigma_{31}^j & \sigma_{32}^j & \sigma_{33}^j \end{bmatrix} \begin{bmatrix} cos\theta & -sin\theta & 0 \\ sin\theta & cos\theta & 0 \\ 0 & 0 & 1 \end{bmatrix}$$

Therefore, the normal stress in the x_3 direction (the set of target points are called I2) due to A_1, A_2, A_3 & A_4 source strength vectors can be written as:

$$s11_{I2} = SS11_{21}A_1 + SS11_{22}A_2 + SS11_{23}A_3 + SS11_{24}A_4 \quad (5\text{-}4)$$

Similarly, for shear stresses, from equation (4-96), the following equations can be obtained:

$$s12_{I2} = SS12_{21}A_1 + SS12_{22}A_2 + SS12_{23}A_3 + SS12_{24}A_4 \quad (5\text{-}5)$$

$$s13_{I2} = SS13_{21}A_1 + SS13_{22}A_2 + SS13_{23}A_3 + SS13_{24}A_4 \quad (5\text{-}6)$$

For surface 3, the displacement and stress components are much more complex, as different point sources contributed differently on the displacement and stress

components. So, considering the respective point sources, the displacement and stresses for surface 3 are as follows:

Displacement along normal direction: Surface 3 has a fluid-solid interface. So, at every point at the interface, normal displacement relative to the surface need to be defined such that it satisfies the continuity condition across the surface. If displacements at point x generated by a point source acting at point y is along the x_j direction is denoted by u_{1j}, u_{2j} & u_{3j}, the normal displacement can be written as:

$$u_N = \left(u_{1j}cos\theta + u_{2j}sin\theta\right)cos\varphi - u_{3j}sin\varphi$$

Where θ and φ are angle between x_1& x_2 direction and opening angle respectively.

Using the above equation and equation (4-67), at *I*3 sets of target points, the displacement in the normal direction along inside and outside the surface 3 can be written as:

$$UN_{I3}^{3} = DSN_{31}A_1 + DSN_{32}A_2 + DSN_{33}A_3 + DSN_{34}A_4 \quad (5\text{- }7)$$

$$UN_{I3}^{3'} = DFN_{3W}A_W + DFN_{33^*}A_{3^*} \quad (5\text{- }8)$$

Using equation (4-39) to (4-41) the displacement at any set of target points in the fluid can be calculated as:

$$U3 = DF_{(T1)s}A_s$$

Normal stress: As surface 3 has the nonplaner boundary surface, and for that, at every point of the interface, normal stress relative to the surface need to be defined to satisfy the continuity condition across the surface. When the point source is acting at y in an isotropic solid, the stress develops at point x can be written as follows:

$$\sigma_j = \begin{bmatrix} \sigma_{11}^{j} & \sigma_{12}^{j} & \sigma_{13}^{j} \\ \sigma_{21}^{j} & \sigma_{22}^{j} & \sigma_{23}^{j} \\ \sigma_{31}^{j} & \sigma_{32}^{j} & \sigma_{33}^{j} \end{bmatrix}$$

For this surface, if the opening angle is φ and the angle between x- and y- direction in θ, the transformation matrix at any point x should be:

$$T = \begin{bmatrix} cos\varphi cos\theta & cos\varphi sin\theta & -sin\varphi \\ sin\varphi cos\theta & sin\varphi sin\theta & cos\varphi \\ sin\theta & -cos\theta & 0 \end{bmatrix}$$

Therefore, transformed stresses for point x is:

$$\sigma'^{j} = T\sigma_j T^T$$

$$= \begin{bmatrix} cos\varphi cos\theta & cos\varphi sin\theta & -sin\varphi \\ sin\varphi cos\theta & sin\varphi sin\theta & cos\varphi \\ sin\theta & -cos\theta & 0 \end{bmatrix} \begin{bmatrix} \sigma_{11}^j & \sigma_{12}^j & \sigma_{13}^j \\ \sigma_{21}^j & \sigma_{22}^j & \sigma_{23}^j \\ \sigma_{31}^j & \sigma_{32}^j & \sigma_{33}^j \end{bmatrix} \begin{bmatrix} cos\varphi cos\theta & sin\varphi cos\theta & sin\theta \\ cos\varphi sin\theta & sin\varphi sin\theta & -cos\theta \\ -sin\varphi & cos\varphi & 0 \end{bmatrix}$$

Normal stresses can be calculated at *I*3 target points using equation (4-96)

$$sN_{I3}^3 = SSN_{31}A_1 + SSN_{32}A_2 + SSN_{33}A_3 + SSN_{34}A_4 \quad (5\text{- }9)$$

$$sN_{I3}^{3'} = PF_{3W} + PFN_{33^*}A_{33^*} \quad (5\text{- }10)$$

Following the steps similar to (4-34) to (4-36), the pressure at any sets of target point in the fluid below the plate due to the transducer sources, can be written as:

$$PR_{T1}^S = Q_{(T1)S}A_S$$

Shear stress: Shear stress can also be calculated using the above transformation matrix. At surface 3 can be calculated using equation (4-96):

$$sNN_3' = SSNN_{31}'A_1 + SSNN_{32}'A_2 + SSNN_{33}'A_3 + SSNN_{34}'A_4 \quad (5\text{- }11)$$

$$sN'N_3' = SSN'N_{31}'A_1 + SSN'N_{32}'A_2 + SSN'N_{33}'A_3 + SSN'N_{34}'A_4 \quad (5\text{- }12)$$

For surface 4, the basic equations for displacement and stress will be same as surface 3. Only the transformation angles are different. If the angle between x^m and y^m direction is θ, and the opening angle is φ, then the transformed displacement and stress components can be written as:

$$u_N = \left(u_{1j}cos\theta + u_{2j}sin\theta\right)cos\varphi - u_{3j}sin\varphi$$

$$T = \begin{bmatrix} -sin\varphi cos\theta & -sin\varphi sin\theta & -cos\varphi \\ cos\varphi cos\theta & cos\varphi sin\theta & -sin\varphi \\ sin\theta & -cos\theta & 0 \end{bmatrix}$$

Therefore, transformed stresses for point x is:

$$\sigma^{'j} = T\sigma_j T^T$$

$$= \begin{bmatrix} -sin\varphi cos\theta & -sin\varphi sin\theta & -cos\varphi \\ cos\varphi cos\theta & cos\varphi sin\theta & -sin\varphi \\ sin\theta & -cos\theta & 0 \end{bmatrix} \begin{bmatrix} \sigma_{11}^j & \sigma_{12}^j & \sigma_{13}^j \\ \sigma_{21}^j & \sigma_{22}^j & \sigma_{23}^j \\ \sigma_{31}^j & \sigma_{32}^j & \sigma_{33}^j \end{bmatrix} \begin{bmatrix} -sin\varphi cos\theta & cos\varphi cos\theta & sin\theta \\ -sin\varphi sin\theta & cos\varphi sin\theta & -cos\theta \\ -cos\varphi & sin\varphi & 0 \end{bmatrix}$$

So, for surface 4, the transformed displacement and stress components are as follows:

$$UN_{I4}^4 = DSN_{41}A_1 + DSN_{42}A_2 + DSN_{43}A_3 + DSN_{44}A_4 \quad (5\text{- }13)$$

$$UN_{I4}^{4'} = DFN_{4W}A_W + DSN_{44^*}A_{4^*} \quad (5\text{- }14)$$

$$sN_{I4}^4 = SSN_{41}A_1 + SSN_{42}A_2 + SSN_{43}A_3 + SSN_{44}A_4 \quad (5\text{- }15)$$

$$sN_{I4}^{4'} = PF_{4W} + SSN_{44^*}A_{4^*} \quad (5\text{- }16)$$

$$sNN_4^{'} = SSNN_{41}^{'}A_1 + SSNN_{42}^{'}A_2 + SSNN_{43}^{'}A_3 + SSNN_{44}^{'}A_4 \quad (5\text{- }17)$$

$$sN^{'}N_4^{'} = SSN^{'}N_{41}^{'}A_1 + SSN^{'}N_{42}^{'}A_2 + SSN^{'}N_{43}^{'}A_3 + SSN^{'}N_{44}^{'}A_4 \quad (5\text{- }18)$$

For fluid layer, only A_w & A_3^* point sources are contributing, hence, pressure components measured in this surface is as follows:

$$PR_W^1 = Q5_{WW}A_W \quad (5\text{- }19)$$

$$PR_W^{1'} = Q5_{W3^*} \quad (5\text{- }20)$$

5.3 Boundary and continuity condition

Along surface 1, unit displacement ***V*** is given in the normal direction. So, at this direction, the displacement normal to the interface should be equal to the given displacement and other displacement component must vanish. Then, the displacement condition at surface 1 can be expressed as:

$$DS3_{11}A_1 + DS3_{12}A_2 + DS3_{13}A_3 + DS3_{14}A_4 = V \quad (5\text{-}21)$$

$$DS1_{11}A_1 + DS1_{12}A_2 + DS1_{13}A_3 + DS1_{14}A_4 = 0 \quad (5\text{-}22)$$

$$DS2_{11}A_1 + DS2_{12}A_2 + DS2_{13}A_3 + DS2_{14}A_4 = 0 \quad (5\text{-}23)$$

At surface 2, the normal and shear forces does not have a value due to balanced state:

$$SS11_{21}A_1 + SS11_{22}A_2 + SS11_{23}A_3 + SS11_{24}A_4 = 0 \quad (5\text{-}24)$$

$$SS12_{21}A_1 + SS12_{22}A_2 + SS12_{23}A_3 + SS12_{24}A_4 = 0 \quad (5\text{-}25)$$

$$SS13_{21}A_1 + SS13_{22}A_2 + SS13_{23}A_3 + SS13_{24}A_4 = 0 \quad (5\text{-}26)$$

Also, across the interfaces, the normal stress (**s33**) in solid and fluid media should be continuous and the shear stresses at the interfaces must vanish. Therefore, the equations (5-7) to (5-12) can be written as:

$$DSN_{31}A_1 + DSN_{32}A_2 + DSN_{33}A_3 + DSN_{34}A_4 = DFN_{3W}A_W + DSN_{33^*}A_{3^*} \quad (5\text{-}27)$$

$$SSN_{31}A_1 + SSN_{32}A_2 + SSN_{33}A_3 + SSN_{34}A_{4=}PF_{3W} + SSN_{33^*}A_{33^*} \quad (5\text{-}28)$$

$$SSNN'_{31}A_1 + SSNN'_{32}A_2 + SSNN'_{33}A_3 + SSNN'_{34}A_4 = 0 \quad (5\text{-}29)$$

$$SSN'N'_{31}A_1 + SSN'N'_{32}A_2 + SSN'N'_{33}A_3 + SSN'N'_{34}A_4 = 0 \quad (5\text{-}30)$$

Along surface 4, same boundary and continuity condition exists, and this can be written as:

$$DSN_{41}A_1 + DSN_{42}A_2 + DSN_{43}A_3 + DSN_{44}A_4 = DFN_{4W}A_W + DSN_{44^*}A_{4^*} \quad (5\text{-}31)$$

$$SSN_{41}A_1 + SSN_{42}A_2 + SSN_{43}A_3 + SSN_{44}A_4 = PF_{4W} + PFN_{44^*}A_{4^*} \quad (5\text{-}32)$$

$$SSNN'_{41}A_1 + SSNN'_{42}A_2 + SSNN'_{43}A_3 + SSNN'_{44}A_4 = 0 \quad (5\text{-}33)$$

$$SSN'N'_{41}A_1 + SSN'N'_{42}A_2 + SSN'N'_{43}A_3 + SSN'N'_{44}A_4 = 0 \quad (5\text{-}34)$$

At fluid layer, due to stress free boundary condition:

$$Q5_{WW}A_W = Q5_{W3^*}A_{3^*} \quad (5\text{-}35)$$

Equations (5-21) to (5-35) can be written in the following matrix form:

$$\begin{bmatrix} DS3_{11} & DS3_{12} & DS3_{13} & DS3_{14} & 0 & 0 & 0 \\ DS1_{11} & DS1_{12} & DS1_{13} & DS1_{14} & 0 & 0 & 0 \\ DS2_{11} & DS2_{12} & DS2_{13} & DS2_{14} & 0 & 0 & 0 \\ SS11_{21} & SS11_{22} & SS11_{23} & SS11_{24} & 0 & 0 & 0 \\ SS12_{21} & SS12_{22} & SS12_{23} & SS12_{24} & 0 & 0 & 0 \\ SS13_{21} & SS13_{22} & SS13_{23} & SS13_{24} & 0 & 0 & 0 \\ DSN_{31} & DSN_{32} & DSN_{33} & DSN_{34} & DFN_{3W} & DFN_{33^*} & 0 \\ SSN_{31} & SSN_{32} & SSN_{33} & SSN_{34} & -PF_{3W} & PFN_{33^*} & 0 \\ SSNN'_{31} & SSNN'_{32} & SSNN'_{33} & SSNN'_{34} & 0 & 0 & 0 \\ SSN'N'_{31} & SSN'N'_{32} & SSN'N'_{33} & SSN'N'_{34} & 0 & 0 & 0 \\ DSN_{41} & DSN_{42} & DSN_{43} & DSN_{44} & DFN_{4W} & 0 & DFN_{44^*} \\ SSN_{41} & SSN_{42} & SSN_{43} & SSN_{44} & -PF_{4W} & 0 & PFN_{44^*} \\ SSNN'_{41} & SSNN'_{42} & SSNN'_{43} & SSNN'_{44} & 0 & 0 & 0 \\ SSN'N'_{41} & SSN'N'_{42} & SSN'N'_{42} & SSN'N'_{42} & 0 & 0 & 0 \\ 0 & 0 & 0 & 0 & P5_{WW} & P5_{W3^*} & 0 \end{bmatrix} \begin{Bmatrix} A_1 \\ A_2 \\ A_3 \\ A_4 \\ A_W \\ A_3^* \\ A_4^* \end{Bmatrix} = \begin{Bmatrix} V \\ 0 \\ 0 \\ 0 \\ 0 \\ 0 \\ 0 \end{Bmatrix} \quad (5\text{-}36)$$

Or

$$[MAT]\{\Lambda\} = \{V\} \quad (5\text{-}37)$$

5.4 Solution

The source strength vector $\{\Lambda\}$ of the total system can be calculated from equation (5-37):

$$\{\Lambda\} = [MAT]^{-1}\{V\}$$

After calculating the source strengths, the pressure, velocity, stress and displacement values at any point can be obtained from the equations (5-21) through (5-36).

5.5 Numerical Results

The total ultrasonic pressure field in front of the acoustic lens is generated using the formulation described in the above section. It should be mentioned here, despite the fact that along the central axis of a transducer there are many closed form analytical expressions available; there is no such closed form solution for the total ultrasonic field in front of the transducer. If the source geometry is circular, one can utilize the alternative methods [69, 72-74] that involves summation of a finite number of terms in an infinite series in order to compute the ultrasonic field. Nonetheless, for more complex geometry, there is no existing analytical solution. So, application of a semi- analytical solution like DPSM is unavoidable.

The results for the focused 100 MHz transducer is presented in figure 5-6. The image shows that the beam from the lens first converges at the focal point of the lens curvature, and then the beam diverges beyond the focal point. Very little ultrasonic energy is observed outside of this converging and diverging beam and which is desired.

The maximum strength, represented by the lighter color in figure 5-6, seems to be at the focal point as expected. It can also be observed that the field seems to have an area with high magnitude around the focal point. This phenomenon is particularly valuable, because there could be an extended sweet spot near the focal point where the specimen can be kept. Particularly this is advantageous while focusing the lens on the specimen avoiding tedious and relentless work. Here the sweet spot was found to be 80 µm.

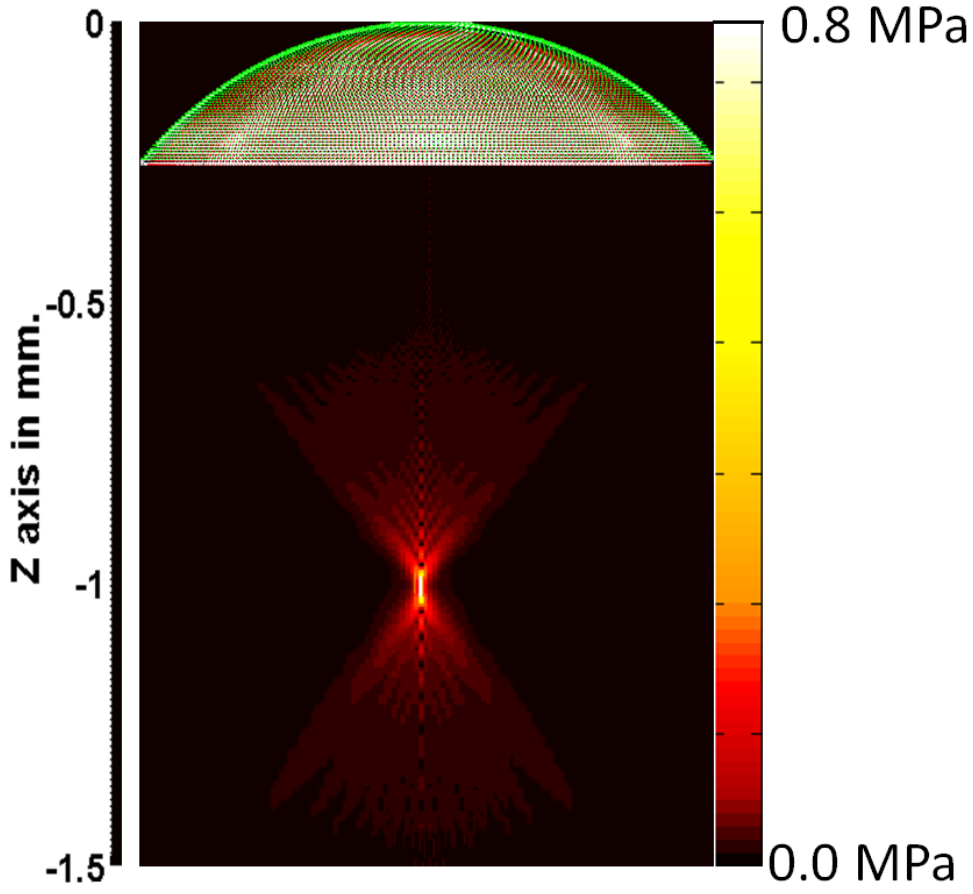

Figure 5.6: Computed pressure field in front of the acoustic lens

The radius of curvature of the lens is 1140 µm. The pressure field variations near (a) 850 µm and (b) the focal point at 1000 µm are shown in figure 5-7. The pressure variations are plotted along the central axis of the acoustic lens.

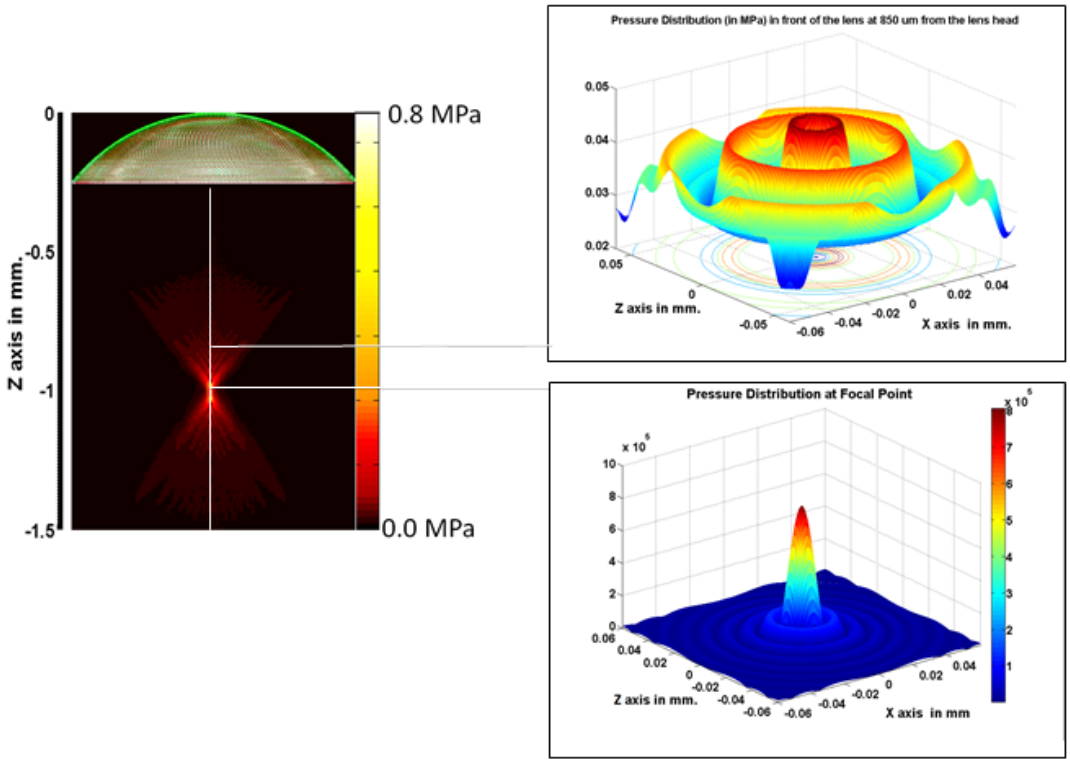

Figure 5.7: Acoustic pressure field variation near (a) 850 µm, (b) focal length.

Figure 5-8 shows the pressure variation plotted along the central axis of the acoustic lens across the z depth. The pressure is nearly 0 when it is close to the lens surface, and the value increases significantly near the focal point. The pressure value is maximum (0.8 MPa) at the focal point (nearly 1000 µm). The acoustic pressure variations near the focal point are shown in figure 5-9. One can see from the plots that the pressure

field is notably strong at the focal point location. The manufacturer PVATepla specified that the 100 MHz acoustic lens manufactured in Germany has a focal length of 1000 μm. The DPSM simulation of the lens has also provided the similar results and thus the computational method is verified. Another method of verification of the pupil function would be calculating the pupil function (assuming a quadratic or cubic polynomial of depth) and through a set of experiments (by incrementally moving the specimen from the focal plane towards the lens) via error minimization of unknown coefficients in the polynomial. However, the later step is omitted from this thesis.

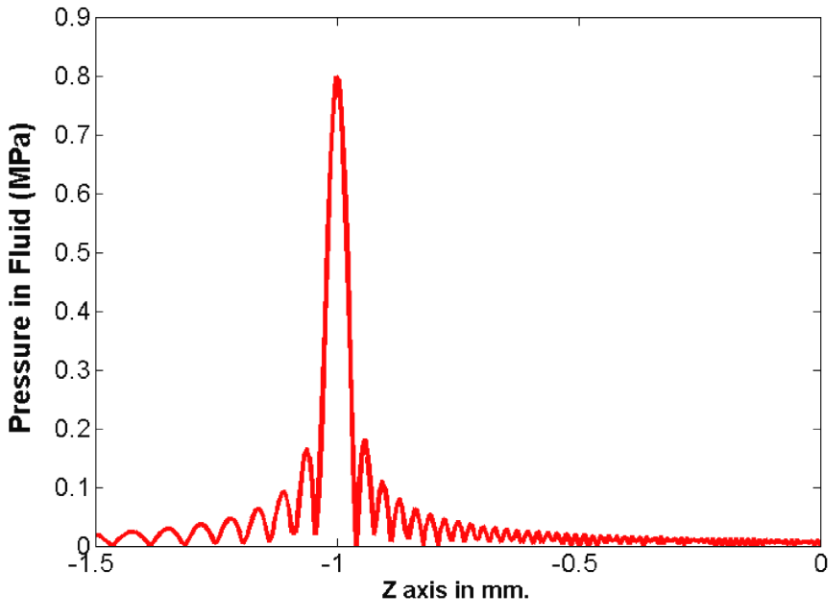

Figure 5.8: Acoustic pressure field variation along z-axis. The peak location suggests the maximum pressure at focal length of the lens

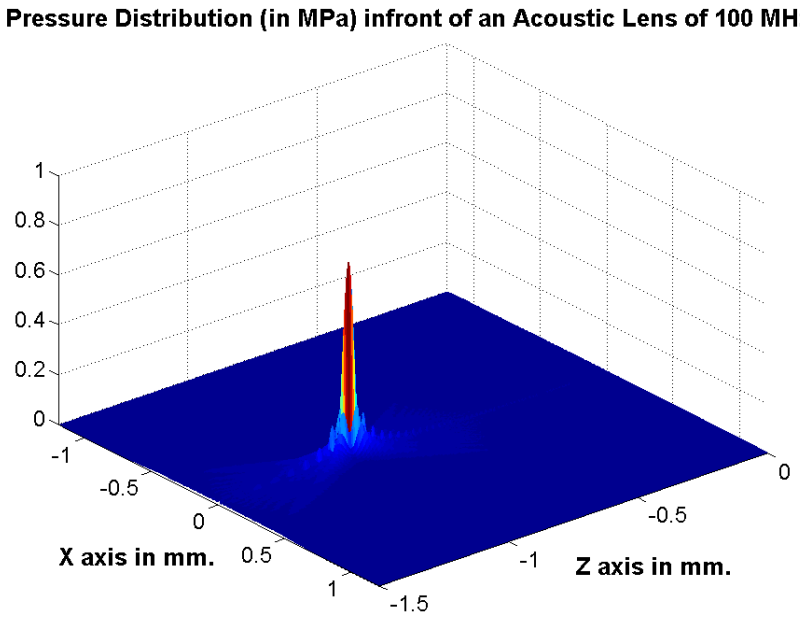

Figure 5.9: Acoustic pressure field variation in the fluid along z-axis. The peak location suggests the maximum pressure at focal length of the lens

5.6 Summary

Previous study on acoustic transducer modelling did not clearly demonstrate the dependence on the generated ultrasonic field on the geometric configurations of the transducer. In this investigation, ultrasonic pressure field in front of an acoustic transducer immersed in a fluid in studied. Here, the boundary conditions are considered similar to the real experimental scenario, and these results can be used to predict the pupil function in front of the acoustic lens.

For this study, a computational model is used to demonstrate a converging ultrasonic beam by a point focus transducer in fluid medium. The problem is modeled by DPSM technique. This technique is able to generate a complete acoustic pressure field in front of a 100 MHz transducer. The numerical result shows special features of the pressure field.

Pressure field variations are presented both at the radius of curvature and at the focal point. From the acoustic pressure field distribution plots, the focal point is very much prominent. The focusing of the beam at the focal point at around 1000 μm closely matched with the vendor specification of the SAM 100 MHz lens and thus the modeling technique is verified.

CHAPTER 6

CONCLUSION

The fundamental objective of the present work is to compute the Pupil function generated by a 100 MHz SAM lens. It is experimentally found that the 100 MHz lens is especially useful for the property determination of the biological material. As the Pupil function cannot be determined experimentally, the only way to compute the PF is the detailed computer simulation. Thus, using the PF, the morphological properties of a pathogen can be determined.

In this dissertation, the detailed development on obtaining the accurate PF in front of an acoustic lens using the DPSM method has been presented. The source strength is given accurately on the transducer position which is located at the top of the surface. The major work was to establish an understanding of the influence of geometry of acoustical lens. The acoustic lens has different geometrical shape, and thus the geometry has played a vital role on the determination of the PF. The basic principle of DPSM as well as how it manifests in mathematical procedures in general are also explained. Using this understanding, the pressure field has been calculated in front of the acoustic lens and it has been found that, the pressure field is accurately focused at the focal point. The peak

pressure at the focal point and the ripple wave effect away from the focal point are also observed.

By obtaining the accurate pupil function for a specific acoustic lens using DPSM (which cannot be determined by other method), the morphomechanical properties of a biological cell can be determined. In this dissertation, accurate PF has been determined, which is the foundation for the understanding of the biological cells. The present work begins the task of developing that fundamental understanding.

REFERENCES

1. Buller, A.H.R., *Research on Fungi,* 1931, London: Green and co.
2. Ingold, C.T., *The biology of fungi,* 1973, Hutchins Education Ltd.
3. Zuber, M.S., et al., *Aflatoxin production in an eight-line dialler of Zea mays infected with Aspergillus flavus.* Phytopathology, 1978. **68**: p. 1346-1349.
4. Moss, S.T., *The Biology of Marine Fungi.*1986, Cambridge, UK.: Cambridge University Press.
5. Carlile, M.J., S.C. Watkinson, and G.W. Gooday, *1 - The Fungi as a Major Group of Organisms*, in *The Fungi (Second Edition)*, M.J. Carlile, S.C. Watkinson, and G.W. Gooday, Editors. 2001, Academic Press: London. p. 1-9.
6. Eaton D. L. and J.D. Groopman, *The Toxicology of Aflatoxins: Human Health, Veterinary, and Agricultural Significance*1994, San Diego, California: Academic.
7. Gow, N.A.R. and G.M. Gadd, *The Growing Fungus*1995: Chapman and Hall.
8. Payne, G.A. and M.P. Brown, *Genetics and physiology of aflatoxin biosynthesis.* Annu Rev Phytopathol, 1998. **36**: p. 329-62.
9. Penalva, M.A. and H.N. Arst, Jr., *Regulation of gene expression by ambient pH in filamentous fungi and yeasts.* Microbiol Mol Biol Rev, 2002. **66**(3): p. 426-46, table of contents.
10. CAST, C.f.A.S.a.T., *Mycotoxins: Risks in Plant Animal and Human Systems*, in *Council for Agricultural Science and Technology.*2003: Ames, Iowa.

11. Bayman, P. and J.L. Baker, *Ochratoxins: a global perspective.* Mycopathologia, 2006. **162**(3): p. 215-23.

12. Yin, Y.N., et al., *Biological control of aflatoxin contamination of crops.* J Zhejiang Univ Sci B, 2008. **9**(10): p. 787-92.

13. Boonen, J., et al., *Human skin penetration of selected model mycotoxins.* Toxicology, 2012. **301**(1-3): p. 21-32.

14. Lobkis, O.I., T. Kundu, and P.V. Zinin, *A theoretical analysis of acoustic microscopy of spherical cavities.* Wave Motion, 1995. **21**(2): p. 183-201.

15. Kundu, T., et al., *Acoustic microscope lens modeling and its application in determining biological cell properties from single- and multi-layered cell models.* J Acoust Soc Am, 2006. **120**(3): p. 1646-54.

16. Wasley, R.J., *Stress Wave Propagation in Solids* ed. J. Miklowitz1973.

17. Rayleigh, J.W.S. and R.B. Lindsay, *The Theory of Sound*1945, New York: Dover Publications.

18. Viktorov, I.A., *Rayleigh and Lamb waves: physical theory and applications.* 1967, New York: Plenum Press.

19. Lamb, H., *On Waves in an Elastic Plate.* Proceedings of the Royal Society of London. Series A, 1917. **93**(648): p. 114-128.

20. Pochhammer, L., *Ueber die Fortpflanzungsgeschwindigkeiten kleiner Schwingungen in einem unbegrenzten isotropen Kreiscylinder*, in *Journal für die reine und angewandte Mathematik (Crelle's Journal)*1876. p. 324.

21. Chree, C., *Longitudinal Vibrations of a Circular Bar.* The Quarterly Journal of Pure and Applied Mathematics, 1886. **21**: p. 287-298.

22. Gazis, D.C., *Three-Dimensional Investigation of the Propagation of Waves in Hollow Circular Cylinders. I. Analytical Foundation.* The Journal of the Acoustical Society of America, 1959. **31**(5): p. 568-573.

23. Gazis, D.C., *Equivoluminal, lamé-type waves in composite hollow cylinders.* International Journal of Solids and Structures, 1976. **12**(6): p. 397-400.

24. McFadden, J.A., *Radial Vibrations of Thick-Walled Hollow Cylinders.* The Journal of the Acoustical Society of America, 1954. **26**(5): p. 714-715.

25. Fung, Y.C. and P. Tong, *Classical and computational solid mechanics*2001, Singapore: World Scientific.

26. Kolsky, H., *Stress waves in solids.* Journal of Sound and Vibration, 1964. **1**(1): p. 88-110.

27. Placko, D. and T. Kundu. *Theoretical study of magnetic and ultrasonic sensors: dependence of magnetic potential and acoustic pressure on the sensor geometry*. 2001.

28. Placko, D., T. Kundu, and R. Ahmad. *Theoretical computation of acoustic pressure generated by ultrasonic sensors in the presence of an interface*. 2002.

29. Placko, D., T. Kundu, and R. Ahmad. *Ultrasonic field computation in the presence of a scatterer of finite dimension*. 2003.

30. Ahmad, R., T. Kundu, and D. Placko, *Modeling of phased array transducers.* J Acoust Soc Am, 2005. **117**(4 Pt 1): p. 1762-76.

31. Banerjee, S. and T. Kundu, *Elastic wave propagation in sinusoidally corrugated waveguides.* The Journal of the Acoustical Society of America, 2006. **119**(4): p. 2006-2017.

32. Banerjee, S., D. Placko, and T. Kundu, *Ultrasonic Field Modeling in Multilayered Fluid Structures Using the Distributed Point Source Method Technique.* Journal of Applied Mechanics, 2005. **73**(4): p. 598-609.

33. Dao, C.M., et al., *Wave propagation in a fluid wedge over a solid half-space – Mesh-free analysis with experimental verification.* International Journal of Solids and Structures, 2009. **46**(11–12): p. 2486-2492.

34. Das, S., et al., *DPSM modeling for studying interaction between bounded ultrasonic beams and corrugated plates with experimental verification.* IEEE Trans Ultrason Ferroelectr Freq Control, 2007. **54**(9): p. 1860-72.

35. Das, S., et al., *Sensors, NDE, and Industrial Applications - DPSM Modeling for Studying Interaction Between Bounded Ultrasonic Beams and Corrugated Plates with Experimental Verification",* , in *IEEE transactions on ultrasonics, ferroelectrics, and frequency control*2007. p. 1860.

36. King, L.V., *On the Acoustic Radiation Field of the Piezoelectric Oscillator and the Effect of Viscosity on Transmission.* Canadian Journal of Forest Research, 1934. **11**: p. 135.

37. Bouwamp, C.J., *Contributions to the Theory of Acoustical Radiation*, in *Philips Research Report*1946. p. 251-277.

38. Schoch, A., *Betrachtungen über das Schallfeld einerKolbenmembran.* Akustische Zeitschrift, 1941. **6**: p. 318-326.

39. Kozina, O.G. and G.I. Makarov, *Transient Processes in the Acoustic Fields Generated by a Piston Membrane of Arbitrary Shaped.* Soviet Physics Acoustics 1961. **7**: p. 39-43.

40. Beaver, W.L., *Sonic nearfields of a pulsed piston radiator.* The Journal of the Acoustical Society of America, 1974. **56**(4): p. 1043-1048.

41. Layton, M.R., et al., *Effects of diffraction on stress pulse propagation.* The Journal of the Acoustical Society of America, 1978. **64**(1): p. 250-256.

42. Miles, J.W., *Transient Loading of a Baffled Piston.* The Journal of the Acoustical Society of America, 1953. **25**(2): p. 200-203.

43. Oberhettinger, F., *On Transient Solutions of the 'Baffled Piston' Problem.* Journal of Research of the National Bureau of Standards, 1961. **65B**: p. 1-6.

44. Robinson, D., S. Lees, and L. Bess, *Near field transient radiation patterns for circular pistons.* Acoustics, Speech and Signal Processing, IEEE Transactions on, 1974. **22**(6): p. 395-403.

45. Stepanishen, P.R., *Transient Radiation from Pistons in an Infinite Planar Baffle.* The Journal of the Acoustical Society of America, 1971. **49**(5B): p. 1629-1638.

46. Stepanishen, P.R., *The Time-Dependent Force and Radiation Impedance on a Piston in a Rigid Infinite Planar Baffle.* The Journal of the Acoustical Society of America, 1971. **49**(3B): p. 841-849.

47. Stepanishen, P.R., *An Approach to Computing Time-Dependent Interaction Forces and Mutual Radiation Impedances between Pistons in a Rigid Planar Baffle.* The Journal of the Acoustical Society of America, 1971. **49**(1B): p. 283-292.

48. Fischer, F.A., *The Radiation of Impulses from Plane Piston Membranes in a Rigid Wall.* Acustica, 1951. **1**: p. 35.

49. Greenspan, M., *Baffled Piston Radiator: Expansion of Potential in Far, Paraxial Field.* The Journal of the Acoustical Society of America, 1966. **40**(1): p. 251-252.

50. Greenspan, M., *Piston radiator: Some extensions of the theory.* The Journal of the Acoustical Society of America, 1979. **65**(3): p. 608-621.

51. McLachlan, N.W., *CIII. The acoustic and inertia pressure at any point on a vibrating circular disk.* Philosophical Magazine Series 7, 1932. **14**(94): p. 1012-1025.

52. Pachner, J., *Pressure Distribution in the Acoustical Field Excited by a Vibrating Plate.* The Journal of the Acoustical Society of America, 1949. **21**(6): p. 617-625.

53. Stenzel, H., *Über die Berechnung des Schallfeldes unmittelbar vor einer kreisförmigen Kolbenmembran.* Annalen der Physik, 1942. **433**(4): p. 245-260.

54. Guptill, E.W., *An Exact Solution of the Acoustical Field Near a Circular Transducer.* The Journal of the Acoustical Society of America, 1952. **24**(6): p. 784-784.

55. Martin, G.E. and J.S. Hickman, *Directional Properties of Continuous Plane Radiators with Bizonal Amplitude Shading.* The Journal of the Acoustical Society of America, 1955. **27**(6): p. 1120-1127.

56. Miner, G.W. and P.A. Laura, *Calculation of the Nearfield Pressure Induced by Vibrating Circular Plates.* The Journal of the Acoustical Society of America, 1967. **42**(5): p. 1025-1030.

57. Papadakis, E.P., *Effects of Input Amplitude Profile upon Diffraction Loss and Phase Change in a Pulse-Echo System.* The Journal of the Acoustical Society of America, 1971. **49**(1B): p. 166-168.

58. Dekker, D.L., R.L. Piziali, and E. Dong, Jr., *Effect of boundary conditions on the ultrasonic-beam characteristics of circular disks.* J Acoust Soc Am, 1974. **56**(1): p. 87-93.

59. Hanish, S., *Chapter III. Theory of Transient Radiation*, in *A Review of World Contributions from 1945 to 1965 to the Theory of Acoustic Radiation*1966, Defense Technical Information Center: Ft. Belvoir.

60. Freedman, A., *Transient Fields of Acoustic Radiators.* The Journal of the Acoustical Society of America, 1970. **48**(1B): p. 135-138.

61. Morse, P.M., *Vibration and Sound.* Noise Control Engineering Journal, 2006. **54**(1): p. 55-58.

62. Sherman, C.H. and D.A. Moran, *Transient Sound Field of Simple Arrays of Circular Pistons*, 1966, Parke Mathematical Labs., Inc., Carlisle, Mass.

63. Chadwick, P. and G.E. Tupholme, *Generation of an Acoustic Pulse by a Baffled Circular Piston.* Proceedings of the Edinburgh Mathematical Society 1966. **15**(4): p. 263-277.

64. Ferris, H.G., *Computation of Farfield Radiation Patterns by Use of a General Integral Solution to the Time-Dependent Scalar Wave Equation.* The Journal of the Acoustical Society of America, 1967. **41**(2): p. 394-400.

65. Tupholme, G.E., *Generation of acoustic pulses by baffled plane pistons.* Mathematika, 1969. **16**(02): p. 209-224.

66. Hasegawa, T., N. Inoue, and K. Matsuzawa, *A new rigorous expansion for the velocity potential of a circular piston source.* The Journal of the Acoustical Society of America, 1983. **74**(3): p. 1044-1047.

67. Spence, R.D., *The Diffraction of Sound by Circular Disks and Apertures.* The Journal of the Acoustical Society of America, 1948. **20**(4): p. 380-386.

68. Carter, A.H. and A.O. Williams, *A New Expansion for the Velocity Potential of a Piston Source.* The Journal of the Acoustical Society of America, 1951. **23**(2): p. 179-184.

69. Douglas Mast, T. and F. Yu, *Simplified expansions for radiation from a baffled circular piston.* The Journal of the Acoustical Society of America, 2005. **118**(6): p. 3457-3464.

70. Wittmann, R.C. and A.D. Yaghjian, *Spherical-wave expansions of piston-radiator fields.* The Journal of the Acoustical Society of America, 1991. **90**(3): p. 1647-1655.

71. Hasegawa, T., N. Inoue, and K. Matsuzawa, *Fresnel diffraction: Some extensions of the theory.* The Journal of the Acoustical Society of America, 1984. **75**(4): p. 1048-1051.

72. Kelly, J.F. and R.J. McGough, *An annular superposition integral for axisymmetric radiators.* J Acoust Soc Am, 2007. **121**(2): p. 759-65.

73. Mellow, T., *On the sound field of a resilient disk in an infinite baffle.* The Journal of the Acoustical Society of America, 2006. **120**(1): p. 90-101.

74. Mellow, T., *On the sound field of a resilient disk in free space.* The Journal of the Acoustical Society of America, 2008. **123**(4): p. 1880-1891.

75. Aarts, R.M. and A.J. Janssen, *On-axis and far-field sound radiation from resilient flat and dome-shaped radiators.* J Acoust Soc Am, 2009. **125**(3): p. 1444-55.

76. Briggs, A., *Acoustic microscopy*1992, NY: Oxford University Press.

77. Maev, R.G., *Scanning Acoustic Microscopy. Physical Principles and Methods. Current Development*, in *Acoustic Microscopy*2009, Wiley-VCH Verlag GmbH & Co. KGaA. p. 9-19.

78. Sokolov, S.Y., *Uses of Ultrasound in Technology and Physics*, 1949, Defense Technical Information Center: Ft. Belvoir.

79. Kessler, L.W., *Review of progress and applications in acoustic microscopy.* The Journal of the Acoustical Society of America, 1974. **55**(5): p. 909-918.

80. Lemons, R.A. and C.F. Quate, *Acoustic microscope-scanning version.* Applied Physics Letters, 1974. **24**(2): p. 163-165.

81. Weise, W., et al., *Imaging of spheres with the confocal scanning optical microscope.* Optics Letters, 1996. **21**(22): p. 1800-1802.

82. Zinin, P., et al., *The theory of three-dimensional imaging of strong scatterers in scanning acoustic microscopy.* Wave Motion, 1997. **25**(3): p. 213-236.

83. D. Crossen, J., et al., *Study of the coating/substrate interface by scanning acoustic microscopy Cathodic disbonding of epoxy-polyamide lacquer from mild steel.* Faraday Discussions, 1997. **107**(0): p. 417-424.

84. Levin, V.M., et al., *Elastic modules of solid C60: measurement and relationship with nanostructure.* Journal of Physics and Chemistry of Solids, 2000. **61**(7): p. 1017-1024.

85. Drescher-Krasicka, E. and J.R. Willis, *Mapping stress with ultrasound.* Nature, 1996. **384**: p. 52-55.

86. Kolosov, O. and K. Yamanaka, *Nonlinear Detection of Ultrasonic Vibrations in an Atomic Force Microscope.* Japanese Journal of Applied Physics Part 2 Letters, 1993. **32**(8A): p. L 1095.

87. Rabe, U. and W. Arnold, *Atomic force microscopy at MHz frequencies.* Annalen der Physik, 1994. **506**(7-8): p. 589-598.

88. Liebeaux, N. and D. Placko, *DPSM Formulation for Basic Magnetic Problems*, in *DPSM for Modeling Engineering Problems*2006, John Wiley & Sons, Inc. p. 231-245.

89. Schmerr, L.W., *Fundamentals of ultrasonic nondestructive evaluation : a modeling approach*1998, New York: Plenum Press.

90. Mal, A.K. and S.J. Singh, *Deformation of elastic solids*1991, New Jersey: Prentice Hall.

91. Korpel, A., L.W. Kessler, and P.R. Palermo, *Acoustic Microscope operating at 100 MHz.* Nature, 1971. **232**(5306): p. 110-111.

92. Yu, Z. and S. Boseck, *Scanning acoustic microscopy and its applications to material characterization.* Reviews of Modern Physics, 1995. **67**(4): p. 863-891.

93. Wickramasinghe, H.K., *Scanning acoustic microscopy: a review.* Journal of Microscopy, 1983. **129**(1): p. 63-73.

94. Hildebrand, J.A. and D. Rugar, *Measurement of cellular elastic properties by acoustic microscopy.* J Microsc, 1984. **134**(Pt 3): p. 245-60.

95. Hildebrand, J.A., et al., *Acoustic microscopy of living cells.* Proc Natl Acad Sci U S A, 1981. **78**(3): p. 1656-60.

96. Kundu, T., J. Bereiter-Hahn, and K. Hillmann, *Measuring elastic properties of cells by evaluation of scanning acoustic microscopy V(Z) values using simplex algorithm.* Biophys J, 1991. **59**(6): p. 1194-207.

97. Kundu, T., J. Bereiter-Hahn, and K. Hillmann, *Calculating acoustical properties of cells: influence of surface topography and liquid layer between cell and substrate.* J Acoust Soc Am, 1992. **91**(5): p. 3008-17.

98. Litniewski, J. and J. Bereiter-Hahn, *Measurements of cells in culture by scanning acoustic microscopy.* J Microsc, 1990. **158**(Pt 1): p. 95-107.

99. Litniewski, J. and J. Bereiter-Hahn, *Acoustic Velocity Determination in Cytoplasm by V(Z) Shift*, in *Acoustical Imaging*, H. Ermert and H.-P. Harjes, Editors. 1992, Springer US. p. 535-538.

Figure 1-1 Reference:

1. http://www.aspergillusflavus.org/aflavus/

2. http://www.nri.org/old/news/archive/newsarchive2003.htm

3. http://www.plantpath.cornell.edu/labs/milgroom/Research_aflatoxin.html

[A] *Introduction to Nondestructive Testing*a, [Homepage of The American Society for Nondestructive Testing], [Online]. Available: http://www.asnt.org/ndt/primer1.htm [2006, August]

[B] *NDT Resource Center: NDT Course Material*b, . Available: http://www.ndt-ed.org/EducationResources/CommunityCollege/communitycollege.htm [2006, August]

[C] *The United States Geological Survey (USGS) Earthquake Hazards Program*c, .

Available: http://earthquake.usgs.gov/ [2006, August]

[D] Available: http://www.olympus-ims.com/data/File/Harrison-UT.en.pdf [2009] [E] Available:

http://www.omegapiezo.com/vibrating_elements_unimorph_equivalent.html [2009] [F] Available: http://www.meas-spec.com/product/t_product.aspx?id=2480# [2009]

APPENDIX A

DIFFERENTIATION OF GREEN'S FUNCTION

Throughout the dissertation, the Green's functions are denoted as follows:

$$ep = \frac{e^{ik_p r}}{r}$$

$$es = \frac{e^{ik_s r}}{r}$$

$$rp = \frac{ik_p}{r} - \frac{1}{r^2} \qquad \text{(A- 1)}$$

$$rs = \frac{ik_s}{r} - \frac{1}{r^2}$$

If we substitute these expressions into equation 4-66, the resultant will be:

$$G_{ij}(x;y) = \frac{1}{4\pi\rho\omega^2}\{ep[k_p^2 R_i R_j + (3R_i R_j - \delta_{ij})rp]\} + \frac{1}{4\pi\rho\omega^2}\{es[k_s^2(\delta_{ij} - R_i R_j) - (3R_i R_j - \delta_{ij})rs]\} \qquad \text{(A- 2)}$$

where, $R_i = \frac{x_i - y_i}{r}$

If the first and second terms on the right hand side of equation A-2 be denoted by Gp_{ij} and Gs_{ij}, then,

$$G_{ijj}(x;y) = Gp_{ij} + Gs_{ij} \qquad \text{(A-3)}$$

$$Gp_{11} = \frac{1}{4\pi\rho\omega^2}\{ep[k_p^2 R_1^2 + (3R_{1^2} - 1)rp]\}$$

$$Gs_{11} = \frac{1}{4\pi\rho\omega^2}\{es[k_s^2(1 - R_{1^2}) - (3R_1^2 - 1)rs]\} \quad \text{(A-4)}$$

$$Gp_{12} = \frac{1}{4\pi\rho\omega^2}\{ep[k_p^2 R_1 R_2 + (3R_1 R_2)rp]\}$$

$$Gs_{12} = \frac{1}{4\pi\rho\omega^2}\{es[k_s^2(-R_1 R_2) - (3R_1 R_2)rs]\} \quad \text{(A-5)}$$

$$Gp_{13} = \frac{1}{4\pi\rho\omega^2}\{ep[k_p^2 R_1 R_3 + (3R_1 R_3)rp]\}$$

$$Gs_{13} = \frac{1}{4\pi\rho\omega^2}\{es[k_s^2(-R_1 R_3) - (3R_1 R_3)rs]\} \quad \text{(A-6)}$$

$$Gp_{22} = \frac{1}{4\pi\rho\omega^2}\{ep[k_p^2 R_2^2 + (3R_{2^2} - 1)rp]\}$$

$$Gs_{22} = \frac{1}{4\pi\rho\omega^2}\{es[k_s^2(1 - R_{2^2}) - (3R_2^2 - 1)rs]\} \quad \text{(A-7)}$$

$$Gp_{23} = \frac{1}{4\pi\rho\omega^2}\{ep[k_p^2 R_2 R_3 + (3R_2 R_3)rp]\}$$

$$Gs_{23} = \frac{1}{4\pi\rho\omega^2}\{es[k_s^2(-R_2 R_3) - (3R_2 R_3)rs]\} \quad \text{(A-8)}$$

$$Gp_{33} = \frac{1}{4\pi\rho\omega^2}\{ep[k_p^2 R_3^2 + (3R_{3^2} - 1)rp]\}$$

$$Gs_{33} = \frac{1}{4\pi\rho\omega^2}\{es[k_s^2(1 - R_{3^2}) - (3R_3^2 - 1)rs]\} \quad \text{(A-9)}$$

So, the combinations that is possible for the $Gp_{ij}\ and\ Gs_{ij}$ can be written as follows:

And

$$Gp_{ij} = Gp_{ji}; Gs_{ij} = Gs\_ji \quad \text{(A-10)}$$

Substituting equations A-4 to A-10 into equation A-3, and then using equation 4-65, the displacement components at an arbitrary point x due to a point force acting at point y can be written as:

$$\begin{aligned} u_1 &= G_{11}P_1 + G_{12}P_2 + G_{13}P_3 \\ u_2 &= G_{21}P_1 + G_{22}P_2 + G_{23}P_3 \\ u_3 &= G_{31}P_1 + G_{32}P_2 + G_{33}P_3 \end{aligned} \tag{A-11}$$

Where, P_1, P_2 & P_3 are the components of the force vector P acting at y. Therefore, the equation 4-65 can be expressed as:

$$u = \begin{Bmatrix} u_1 \\ u_2 \\ u_3 \end{Bmatrix} = \begin{bmatrix} G_{11} & G_{12} & G_{13} \\ G_{21} & G_{22} & G_{23} \\ G_{31} & G_{32} & G_{33} \end{bmatrix} \begin{Bmatrix} P_1 \\ P_2 \\ P_3 \end{Bmatrix} = G(x;y)P \tag{A-12}$$

where

$$G(x;y) = \begin{bmatrix} G_1(x;y) \\ G_2(x;y) \\ G_3(x;y) \end{bmatrix} = \begin{bmatrix} [G_{11} & G_{12} & G_{13}] \\ [G_{21} & G_{22} & G_{23}] \\ [G_{31} & G_{32} & G_{33}] \end{bmatrix} \tag{A-13}$$

And $P = [P_1 \quad P_2 \quad P_3]$

Let, the derivative of a parameter with respect to x_i be denoted by the parameter followed by the letter $d_i, i.e\ rpd_1 = \frac{\partial(rp)}{\partial x_1}$:

$$rpd_1 = \left(\frac{2R_1}{r^3} - \frac{ik_pR_1}{r^2}\right); rsd_1 = \left(\frac{2R_1}{r^3} - \frac{ik_sR_1}{r^2}\right) \tag{A-14}$$

$$rpd_2 = \left(\frac{2R_2}{r^3} - \frac{ik_pR_2}{r^2}\right); rsd_2 = \left(\frac{2R_2}{r^3} - \frac{ik_sR_2}{r^2}\right) \tag{A-15}$$

$$rpd_3 = \left(\frac{2R_3}{r^3} - \frac{ik_pR_3}{r^2}\right); rsd_3 = \left(\frac{2R_3}{r^3} - \frac{ik_sR_3}{r^2}\right) \tag{A-16}$$

R_i is defined below equation A-2.

Let $eo_{ij} = R_iR_j$ and $et_{ij} = 3eo_{ij} = 3R_iR_j$, then, the differentiation od the equations can be expressed as:

$$eo_{ii}d_i = -\frac{2R_i^3}{r} + \frac{2R_i}{r}; eo_{ij}d_i = -\frac{2R_i^2R_j}{r} + \frac{R_j}{r} = eo_{ji}d_i \tag{A-17}$$

$$eo_{ij}d_k = -\frac{2R_iR_jR_k}{r}; eo_{ii}d_j = -\frac{2R_i^2R_j}{r} \tag{A-18}$$

$$et_{ii}d_i = -\frac{6R_i^3}{r} + \frac{26}{r}; et_{ij}d_i = -\frac{6R_i^2R_j}{r} + \frac{3R_j}{r} = et_{ji}d_i \tag{A-19}$$

$$et_{ij}d_k = -\frac{6R_iR_jR_k}{r}; et_{ii}d_j = -\frac{6R_i^2R_j}{r} \tag{A-20}$$

The repeated index in the above expressions does not imply summation.

Differentiating the terms Gp_{ij} & Gs_{ij} (equations A-4 to A-10) with respect to x_i and substituting equations A-14 to A-20 into the differentiations, the following equations can be obtained:

$$Gp_{ii}d_i = \frac{1}{4\pi\rho\omega^2}\{ep[k_p^2eo_{ii}d_i + (-1 + et_{ii})rpd_i + rp(et_{ii}d_i)]\} + Gp_{ii}\left(ik_pR_iep - \frac{R_iep}{r}\right) \tag{A-21}$$

$$Gs_{ii}d_i = \frac{1}{4\pi\rho\omega^2}\{es[k_s^2eo_{ii}d_i - (-1 + et_{ii})rsd_i + rs(et_{ii}d_i)]\} + Gs_{ii}\left(ik_sR_ies - \frac{R_ies}{r}\right) \tag{A-22}$$

$$Gp_{ii}d_j = \frac{1}{4\pi\rho\omega^2}\{ep[k_p^2 eo_{ii}d_j + (-1+et_{ii})rpd_j + rp(et_{ii}d_j)]\} + Gp_{ii}\left(ik_pR_jep - \frac{R_jep}{r}\right)$$

(A-23)

$$Gs_{ii}d_j = \frac{1}{4\pi\rho\omega^2}\{es[-k_s^2 eo_{ii}d_j - (-1+et_{ii})rsd_j + rs(et_{ii}d_j)]\} + Gs_{ii}\left(ik_sR_jes - \frac{R_jes}{r}\right)$$

(A-24)

$$Gp_{ij}d_i = \frac{1}{4\pi\rho\omega^2}\{ep[k_p^2 eo_{ij}d_i + (et_{ii})rpd_i + rp(et_{ij}d_i)]\} + Gp_{ij}\left(ik_pR_iep - \frac{R_iep}{r}\right)$$

(A-25)

$$Gs_{ij}d_i = \frac{1}{4\pi\rho\omega^2}\{es[k_s^2 eo_{ij}d_i - (et_{ii})rsd_i + rs(et_{ij}d_i)]\} + Gs_{ij}\left(ik_sR_ies - \frac{R_ies}{r}\right)$$

(A-26)

$$Gp_{ji}d_i = \frac{1}{4\pi\rho\omega^2}\{ep[k_p^2 eo_{ji}d_i + (et_{ji})rpd_i + rp(et_{ji}d_i)]\} + Gp_{ji}\left(ik_pR_iep - \frac{R_iep}{r}\right)$$

(A-27)

$$Gs_{ji}d_i = \frac{1}{4\pi\rho\omega^2}\{es[k_s^2 eo_{ji}d_i - (et_{ji})rsd_i + rs(et_{ji}d_i)]\} + Gs_{ji}\left(ik_sR_ies - \frac{R_ies}{r}\right)$$

(A-28)

$$Gp_{ij}d_k = \frac{1}{4\pi\rho\omega^2}\{ep[k_p^2 eo_{ij}d_k + (et_{ii})rpd_k + rp(et_{ij}d_k)]\} + Gp_{ij}\left(ik_pR_kep - \frac{R_kep}{r}\right)$$

(A-29)

$$Gs_{ij}d_k = \frac{1}{4\pi\rho\omega^2}\{es[k_s^2 eo_{ij}d_k - (et_{ii})rsd_k + rs(et_{ij}d_k)]\} + Gs_{ij}\left(ik_sR_kes - \frac{R_kes}{r}\right)$$

(A-30)

In addition, from equation A-3, the differentiation of the displacement Green's function can be written as:

$$G_{ii}d_i = Gp_{ii}d_i + Gs_{ii}d_i \tag{A-31}$$

$$G_{ii}d_i = Gp_{ii}d_j + Gs_{ii}d_j \tag{A-32}$$

$$G_{ij}d_i = Gp_{ij}d_i + Gs_{ij}d_i \tag{A-33}$$

$$G_{ji}d_i = Gp_{ji}d_i + Gs_{ji}d_i \tag{A-34}$$

$$G_{ij}d_k = Gp_{ij}d_k + Gs_{ij}d_k \tag{A-35}$$

As stated earlier, repeated indices in equation A-21 to A-35 does not imply summations.

The stress components (σ_{ij}) at any point x generated by a concentrated force of unit amplitude acting at any point y in the x_m direction can be denoted by σ_{ij}^m and each component can be expressed as:

$$\sigma_{11}^1 = (2\mu + \lambda)(G_{11}d_1) + \lambda(G_{21}d_2 + G_{31}d_3) \tag{A-36}$$

$$\sigma_{11}^2 = (2\mu + \lambda)(G_{12}d_1) + \lambda(G_{22}d_2 + G_{32}d_3) \tag{A-37}$$

$$\sigma_{11}^3 = (2\mu + \lambda)(G_{13}d_1) + \lambda(G_{23}d_2 + G_{33}d_3) \tag{A-38}$$

$$\sigma_{33}^1 = (2\mu + \lambda)(G_{31}d_3) + \lambda(G_{11}d_1 + G_{21}d_2) \tag{A-39}$$

$$\sigma_{33}^2 = (2\mu + \lambda)(G_{32}d_3) + \lambda(G_{12}d_1 + G_{22}d_2) \tag{A-40}$$

$$\sigma_{33}^3 = (2\mu + \lambda)(G_{33}d_3) + \lambda(G_{13}d_1 + G_{23}d_2) \tag{A-41}$$

$$\sigma_{31}^{1} = \mu(G_{31}d_1 + G_{11}d_3) \quad \text{(A-42)}$$

$$\sigma_{31}^{2} = \mu(G_{32}d_1 + G_{12}d_3) \quad \text{(A-43)}$$

$$\sigma_{31}^{3} = \mu(G_{33}d_1 + G_{13}d_3) \quad \text{(A-44)}$$

$$\sigma_{32}^{1} = \mu(G_{31}d_2 + G_{21}d_3) \quad \text{(A-45)}$$

$$\sigma_{32}^{2} = \mu(G_{32}d_2 + G_{22}d_3) \quad \text{(A-46)}$$

$$\sigma_{32}^{3} = \mu(G_{33}d_2 + G_{23}d_3) \quad \text{(A-47)}$$